THE UNIVERSITY OF MICHIGAN

INDUSTRY PROGRAM OF THE COLLEGE OF ENGINEERING

PRESSURE GRADIENTS ASSOCIATED WITH NON-ADIABATIC TWO-PHASE FLOW

V. Lemi Ulugol

January, 1961

IP-490

ACKNOWLEDGMENT

The author wishes to express his gratitude to Dr. John A. Clark, Professor-in-charge of the Heat Transfer and Thermodynamics Laboratory, for his continual encouragement and guidance throughout the course of the present investigation.

The author also expresses his appreciation to Professor Gordon J. Van Wylen, Chairman of the Mechanical Engineering Department, for his interest and the cooperation received from the Department in the allocation of the equipment, instruments and space.

The financial assistance of the University of Michigan Research Institute is also gratefully acknowledged.

The cooperation of Mr. Waldemar Salva, Laboratory technician and of the other laboratory personnel is highly appreciated.

The assistance of Mrs. Norlene Martin and the cooperation of the Industry Program of the College of Engineering in the preparation of the manuscript also is highly appreciated.

The appointment held during the period of this research and supported by the International Cooperation Administration under the Visiting Research Scientists Program administered by the National Academy of Sciences of the United States of America, is gratefully acknowledged.

TABLE OF CONTENTS

LIST OF FIGURES

LIST OF FIGURES CONT'D

NOMENCLATURE

A	Heat transfer area, sq. ft.
D	Diameter, in.
E	Voltage, volts
f	Friction factor
G	Mass velocity, lb/hr ft^2
h	Enthalpy, Btu/lb
I	Current, Amps
k	Thermal conductivity Btu/hr ft degF.
L	Length of the test section, in.
l	Distance from test section inlet, in.
m, n	Coefficients in equation (14)
N_{Re}	Reynolds number
P	Pressure (lb/sq in or in.-wat.)
ΔP, Δh	Pressure drop
$\left(\frac{dP}{dl}\right)_{TP}$	Pressure gradient for two-phase flow
$\left(\frac{dP}{dl}\right)_{0}$	Pressure gradient for liquid flow
q	Heat Input, Btu/hr
q/A	Heat flux, Btu/hr sq ft
$R = \frac{(dP/dl)TP}{(dP/dl)_0}$	Pressure gradient ratio
r	Radius, in.
T	Temperature, deg F
ΔT	Temperature difference, deg F
U	Velocity, ft/sec
V	Specific volume, ft^3/lb
W	Flow rate (lb/hr or gpm)

x	Steam quality
μ	Dynamic viscosity (cp)
χ	Dimensionless parameter defined by Equation (7)

Subscripts

ACT	Actual flow
FOG	Fog flow
SEP	Separated flow
g	Steam
l	Saturated liquid
in	Inlet
o	Inside
w	Outside
ts	Test section
TP	Two-phase

SUMMARY

Pressure drop and wall temperature data have been obtained during forced-circulation boiling of water in an electrically heated horizontal tube at substantially atmospheric pressure. The test section was a 0.750 in O.D. by 0.620 in. I.D. stainless steel tube. The heat generation was accomplished by passing the electric current through the test section.

Local pressure gradients were determined for a range of mass flow rates and steam qualities using heat flux values up to 225,000 Btu/hr ft^2. Two different heat transfer and flow regions, designated as "nucleate boiling region" and "liquid-dispersed region" were distinguished. The value of the steam quality corresponding to the suggested transition point between these regions was found to be almost inversely proportional to the mass velocity. An empirical equation for the pressure gradients in the liquid dispersed region is given as a function of the steam quality.

Some local wall temperature measurements are presented. The high-speed still pictures of the steam-water mixture at the outlet of the test section also are presented.

I. INTRODUCTION

A. Statement of the Problem

During the last two or three decades considerable research has been devoted to the problem of the co-current flow of gas-liquid or vapor-liquid systems in tubes. Such flow systems are encountered in many branches of industry, such as petroleum production and refining, steam generation, refrigeration etc. Recent growing interest in single-component two-phase nonadiabatic systems results from their association with the heat removal from the nuclear reactors and rocket motors. Since the relative mass flow rates in steady flow of both phases are a function of the position along the tube, this type of flow is the most difficult to investigate experimentally and to analyze. The main problems involved include the flow stability, the pressure drop characteristics, the vapor-liquid distribution and holdup, the heat transfer rates and burnout or the maximum heat flux.

Owing to the relative complexity of the problem, very little progress has been made toward understanding the processes involved in progressive vaporization of a fluid along a tube. One of the main difficulties is that several flow patterns of widely different geometry may exist depending upon the position of the confining conduit and the interplay of the relevant forces, such as gravitational, intraphase and interphase forces. The descriptions of the two-phase flow patterns are available in the literature (1,2,3,4)*. The behavior of the system is closely associated with the type of flow pattern which occurs. Consequently, for an analysis of boiling inside tubes, it is of primary importance to study the variation of the point or local conditions along

the tube, including the pressure, the axial pressure gradient, the wall temperature, the fluid temperature and the liquid and vapor holdup. The information gathered through experimental investigations directed at a study of the above conditions will be helpful in framing appropriate physical models and thus will make possible a sound analytical approach to the several aspects of the problem. Not until quite recently have studies of the local conditions during boiling inside tubes been published.

Dengler (5) in 1952 and Dengler and Addoms (6) in 1956 presented data for local pressure gradients and local film heat transfer coefficients for vaporization of water in a vertical tube at low pressures and over the entire steam quality range of 0 to 100 percent.

Querrieri and Talty (7) published a study of heat transfer to a number of organic liquids boiling in two single tube natural circulation vertical evaporators.

Jakob, Leppert and Reynolds (8) presented pressure drop data during forced circulation boiling of water in an electrically heated horizontal tube at operating pressures between 30 and 200 psia. Empirical correlations were given for the over-all static pressure drop and the local pressure gradient as a function of the weight fraction evaporated and the absolute system pressure.

Mumm (9) investigated the heat transfer characteristics of the system described in reference (8).

---

* Numbers in parentheses refer to the bibliography at the end.

McNelly and Coulson (10) in a study of the performance of the climbing film evaporators, confirmed the successive change of the flow conditions along the tube and distinguished between three different mechanisms of heat transfer as taking place in the evaporator.

Bennett, Collier, Pratt and Thornton (11) have published the local heat transfer and pressure drop data for a vertical steam-water flow in an annulus at approximately atmospheric pressure.

B. Present Work

In view of the foregoing, an experimental investigation of the local conditions of pressure and temperature was undertaken using a steam-water system at substantially atmospheric pressure. Water which was preheated to approximately the saturation condition was introduced into an electrically heated test section. This consisted of a horizontal stainless steel tube (0.750 in O.D., 0.620 in. I.D., 50 inches long) and the heat generation was accomplished by passing the electric current through the test section itself. This tube simulates systems having internal heat generation in the walls such as heterogeneous nuclear reactor coolant channels.

The over-all pressure drop, the local pressure gradients, and the local wall temperatures at the lower and upper portions of the tube were determined for a range of mass flow rates and steam qualities, using heat flux up to 225,000 BTU/hr-ft^2. Mass velocity was varied from 1.38 x 10^5 lb/hr ft^2 to 4.14 x 10^5 lb/hr ft^2 and the maximum weight fraction evaporated was about 50%. A photographic study of the steam-water mixture at the outlet of the test section also was included. Photographs were taken with a 4 in. x 5 in. camera

used with a strobe-light unit. Also motion pictures of the outcoming mixture were taken with a 16mm camera at a speed of 300 frames/second.

II. EXPERIMENTAL APPARATUS AND INSTRUMENTATION

For the purpose of the present study, the equipment which is described below was designed, built, and used in the Heat Transfer and Thermodynamics Laboratory of the Mechanical Engineering Department.

A. General Description of the Equipment

A schematic diagram and an over-all view of the equipment are shown in Figures 1 and 2. Figure 3 shows a close-up of the instruments. A once-through system was used because of its relative simplicity with the Ann Arbor City water as the water supply. During the preliminary runs water was taken direct from the Laboratory lines but the pressure fluctuations proved to be unsatisfactory. The subsequent use of a centrifugal pump has permitted the maintenance of steady inlet conditions for the system. The water which was pumped from a water tank passed through an ion exchanger and two filters which were incorporated to prevent the contamination of the test section surface. A pressure regulating valve was used in conjunction with a needle valve for flow adjustments.

The flow rate was measured by both a calibrated orifice and by a turbine type flowmeter. Preheating was accomplished by a series of immersion type electric heaters placed in $2\frac{1}{2}$ in. brass pipes, having a total rating of 40 KW. By means of several on-off switches and a 3KVA Variac the pre-heating capacity could be adjusted continuously in the range of 0-40KW. Air bleeding cocks were provided at the highest points of the pre-heater connections. A second flowmeter was placed immediately upstream of the test section for monitoring the fluctuations in the flow. The test section was insulated electrically from the rest of the equipment.

The tube used as the test section was a 0.750 in O.D. by 0.620 in. I.D., type 304, seamless stainless steel tube. The total length of the tube was 7 feet, with an unheated hydrodynamic starting length having an L/D of 45, and a heated length of 50 inches. The internal heat generation was accomplished by passing the electric current through the test section itself. For this purpose current leads were attached to the copper lugs silver soldered at each end of the test section. Power was supplied from a 50 KW, 25V D.C., 2000 A germanium rectifier unit. This power was subject to remote manual and automatic control and regulation.

The bulk temperature of water entering the test section was measured by means of a pre-calibrated 30-gage copper-constantan thermocouple which was immersed in the water stream.

The details of the test section are shown in Figure 4. Ten pressure taps spaced 5 inches apart were located along the test section and two other pressure taps were provided before and after the test section. Each pressure tap consisted of one inch length of 1/8 in O.D. by 1/16 in. I.D. stainless steel tubing, silver-soldered to the test section. A 1/32 inch radial hole was drilled through the wall of the test section at each pressure tap location. The pressure taps were connected, by means of Tygon tubing, to a 13-tube common-reservoir type manometer, which premitted the measurement of the pressure drop as well as the pressure at the inlet of the test section.

One horizontal and one vertical thermocouple probe were placed in four cross-sections at 10, 25, 40 and 49 inches from the inlet of the test section, for the measurement of the fluid temperatures.

The position of each thermocouple in the tube was controlled by a micrometer adjustment system.

For the measurement of the outside tube wall temperatures, twenty thermocouples were placed at the top and bottom of the tube at several stations. From the measured outside wall temperatures, inside wall temperatures were calculated considering the radial temperature difference across the wall of the resistance heated tube.

A drain tank was used to receive the discharge from the test section and a spray of water was provided for reducing the amount of steam escaping to the atmosphere. Since the test section outlet was open to the atmosphere, the discharging steam-water mixture could be visually observed.

All pipework and valve material was either stainless steel or brass. The part of the equipment extending from the preheater inlet to the test section outlet was thoroughly insulated with $2\frac{1}{4}$ in. thick fiberglass blanket insulation.

B. Instrumentation

1. Measurement of the Flow Rate

An orifice and a turbine type flowmeter were used for the measurement of the flow rate.

a. Orifice

Two orifice plates of 0.218 in. and 0.312 in diameters were used for the range of flow rate studied. Each orifice had been previously calibrated by means of a weigh tank, and the calibration was checked at regular intervals. No deviation from the original calibration was detected. The calibration curves for both orifices are shown

in Figures 5 and 6. As seen from these curves, the orifice diameters used made it possible to have a differential pressure range which could be read with good accuracy. A 100-inch inverted-U-type manometer was used for measuring the differential pressure across the orifice. An adjustable air pressure was applied at the top of the water columns. The pressure on the upstream side of the orifice was also applied to a reservoir-type mercury manometer open to the atmosphere. The indication of this manometer reflected the constancy of the flow through the equipment.

b. Flowmeter

A Waugh turbine type flowmeter (Model No. FL-8S) was used. This flowmeter measures the fluid flow by determining the fluid velocity in a passage containing a freely spinning turbine wheel. The passage of the fluid results in the rotation of the turbine wheel at a speed proportional to the flowrate. As the turbine rotates, electrical pulses are generated in the externally mounted coil assembly. The frequency of the generated pulses is directly proportional to the flowrate. The calibration curve for this flowmeter is shown in Figure 7.

After proper pre-amplification the output of the flowmeter was fed to a Model 522B Hewlett-Packard Electronic counter.

In all cases the flow rate values measured with the orifice and the flowmeter were essentially the same. And it is believed that the mass flow rates are correct within $\pm$ 1%.

2. Flow rate Recording

In addition to the readings of the electronic counter, a record of the flow rate as a function of time was considered desirable from the standpoint of a better analysis of the system performance.

Besides measuring the frequency of the pulses generated by the flowmeter as an indication of the flow rate, the voltage of these pulses was used to obtain such a record. Figure 8 shows a plot of the peak-to-peak voltage of the pulses, as measured with an oscilloscope and a voltage calibrator, versus the flow rate. It is seen that this voltage is also proportional to the flow rate within close approximation. Consequently a simple rectifying circuit was incorporated in order to obtain a D.C. voltage which would be proportional to the flow rate. And this D.C. voltage was fed to one channel of a direct recording multiple channel Visicorder oscillograph.

This flowmeter was placed at the inlet side of the equipment. A second flowmeter of the same type was placed just before the test section. This location was considered to be more suitable for evaluating fluctuations in the flow, since it offered a much smaller damping for any possible flow oscillation occurring in the test section.

A diagram of the electrical circuit used for the measurement and recording of the flow rate with these flowmeter is given in Figure 9.

3. Measurement of the Electrical Power Input to the Test Section.

The power dissipated in the test section was determined by measuring the voltage drop across the test section and the current passing through it.

For the test section voltage drop measurement voltage taps were taken directly from the ends of the test section and a voltage-divider network was used as illustrated in Figure 10. The voltage-divider network consisted of a 50 KΩ and a 25 Ω precision wire wound resistor in series. The voltage drop across the 25Ω resistor was

measured with a Leeds & Northrup Model 8662 portable precision potentiometer. The voltage drop across the test section is then

$$E_{ts} = E_1 \left(\frac{R_1 + R_2}{R_1}\right) \qquad (1)$$

The electric current was determined from the measured voltage drop across a 25×10^{-6} Ω calibrated shunt which was in series with the test section. The same portable precision potentiometer was used for this measurement.

4. Measurement of the temperatures

a. Fluid Temperatures

For the measurement of the test section inlet temperature and of the fluid temperatures in the test section, pre-calibrated 30-gage copper-constantan thermocouples were used. Previous use of the iron-constantan thermocouples had not been satisfactory owing to the rapid corrosion of the bare thermocouple tips.

The emf of these thermocouples were read with a Leeds-Northrup portable precision potentiometer. In addition, provisions had been made for feeding them to a multiple-channel direct recording Minneapolis-Honeywell Model 1012 "Visicorder" oscillograph which would make it possible to have simultaneous time recordings of the fluid temperatures.

b. Wall Temperatures

The outside wall temperatures were measured by precalibrated 30-gage iron-constantan thermocouples which were attached to the outside tube surface. These thermocouples were insulated from the tube wall by a thin sheet of mica of 0.0015 in. thick and held to the tube

surface by high temperature glass electrical tape and asbestos cord. In order to keep the thermal errors from axial conduction to a minimum each thermocouple was wrapped around the tube one quarter turn before it was led out through the insulation.

In addition to reading the emf of these thermocouples with a portable precision potentiometer, a 20-point (adjustable zero, adjustable range) Leeds-Northrup Speedomax temperature recorder was used to obtain chart recordings.

5. Static Pressure Measurements

For measurement of the static pressure along the test section, a 13-tube 60-inch common-reservoir type manometer was used. The pressure taps were connected to the manometer tubes, by Tygon tubing, as shown in Figure 11. The pressure at the first pressure tap was applied to the manometer reservoir and to the tube no. 12 (starting from the left side) and was used as a reference pressure for all pressure readings. Thus, the height of the indicating liquid in any one tube above the indicating liquid level in the tube no. 12 corresponded to the pressure drop between the first and the considered pressure taps. The last manometer tube was left open to the atmosphere so that it would indicate the gage pressure at the first pressure tap. Mercury and an indicating liquid having a specific gravity of 1.75 were used in the manometer, for different pressure drop ranges.

The manometer used was a photo-manometer with translucent scales and built-in backlighting which could permit photographing the manometer columns. However, in view of the steadiness of the flow and of the pressure values observed during the experiments, a recourse to photography was unnecessary.

C. Experimental Procedure

At the beginning of each run, a constant flow rate was set by means of the flow control valve, the preheater power was turned on and the pre-heating capacity was adjusted to obtain the desired test section inlet temperature. Then the power was applied to the test section, and a re-adjustment was made on the flow rate to maintain it at the originally set value.

Steady state conditions were established, for each run and held for a period of one hour before recording the data. During this one hour period four sets of flow rate, pressure and temperature readings were taken for checking the uniformity and steadiness of the flow.

Re-runs were made periodically to check the reproducibility of the experimental results.

D. Data Reduction Method

1. In the reduction of the recorded experimental results, the following assumptions were made:

-Thermodynamic equilibrium between the phases exists at each point along the tube.

-The generation of electrical heat in the tube wall is uniform, and the thermal conductivity and electrical resistivity properties of the tube material are constant radially and axially along the length of the tube. (Maximum tube wall ΔT was $60^{\circ}F$)

-Vapor formation starts at the point where the fluid enthalpy becomes equal to the local saturated liquid enthalpy.

-Steam quality (mass fraction evaporated) is calculated by a heat balance.

2. Using these assumptions, the following is a description of the data reduction procedure:

-From the pressure drop measurements the pressure profile along the test section is determined.

-Fluid enthalpy (h_{in}) at the test section inlet is known from the measured inlet temperature (T_{in}).

-From the measured test section voltage drop (E_{ts}) and the current (I), the electrical power input to the test section is known. The heat loss from the test section is estimated as 1% of the total heat input. The heat transfer area (A) is defined by the inside surface of the test section. Therefore the heat flux (q/A) may be computed as follows:

$$q/A = \frac{0.99 \times 3.413 \; E_{ts} \; I}{A} \quad Btu/hr.ft^2 \tag{2}$$

where

$$A = \pi \; D_o \; L$$

$$A = \pi \; \frac{0.62}{12} \cdot \frac{50}{12} = 0.676 \text{ sq. ft.}$$

consequently

$$q/A = 5 \; E_{ts} \; I \quad Btu/hr.ft^2 \tag{3}$$

-From the known heat input (q) to the test section, the increase of the fluid enthalpy per unit length along the test section is known. Therefore at any point along the test section, the enthalpy of the two-phase mixture can be calculated as,

$$h_{tp} = h_{in} + \frac{q}{WL} \; l \quad Btu/lb \tag{4}$$

-Point steam qualities are calculated as

$$X \; \% = \frac{h_{tp} - h_l}{h_{lg}} \times 100\% \tag{5}$$

where h_l and h_{lg} are the saturated liquid and the evaporation enthalpies corresponding to the pressure to the pressure at the point in consideration.

-From the measured outside wall temperatures (T_w), inside wall temperatures (T_o) are calculated considering the radial temperature difference across the wall of the resistance heated tube. The differential equation governing the temperature distribution in an electrically heated circular tube with temperature-dependent properties of thermal conductivity and electrical resistivity was originally solved by Kreith and Summerfield (12). An interesting solution from the standpoint of a hand calculation was presented by Clark (13) for the case of temperature-dependent properties and with outward heat flow. For the present case of inward heat flow using the same procedure and assuming constant properties for the wall material a similar and simplified form was derived. This equation is,

$$T_w - T_o = \frac{q}{A} \cdot \frac{r_o}{k} \left[\frac{r_w^2}{r_w^2 - r_o^2} \text{ Ln } \frac{r_w}{r_o} - \frac{1}{2} \right] \qquad (6)$$

III. EXPERIMENTAL RESULTS

The experimental work reported herein was limited to the following range of variables:

1. System: 0.750 in. O.D., 0.620 in. I.D. horizontal tube
2. Mass velocity, $G = 1.38 \times 10^5 - 4.14 \times 10^5$ lb/hr ft^2 corresponding to inlet velocity, $U_{in} = 0.64 - 1.92$ ft/sec
3. Test section inlet temperature, $T_{in} = 205^{\circ}F$ corresponding to inlet Reynolds number, $N_{Re} = 10^4 - 3 \times 10^4$
4. Heat flux, q/A = up to 2.25×10^5 BTU/hr ft^2
5. Bulk steam quality (mass fraction), x: up to 50.5%
6. Pressure, P = substantially atmospheric pressure

A. Flow Steadiness

Except the runs with low exit qualities the flow through the test section was found to be essentially steady, as indicated by the turbine type flowmeter. The lower limit of the steady flow range corresponded to an exit quality of about 7% for the minimum mass velocity used which was 1.38×10^5 lb/hr-ft^2, and to smaller qualities with increasing flow rates.

The unsteady flow condition consisted mainly in a pulsating stratified flow with alternate slugs of liquid and vapor.

Pictures were taken for both the steady and unsteady flow conditions and are presented in the section dealing with the photographic study of the outlet mixture.

B. Adiabatic Pressure Drop

For the purpose of comparing the adiabatic pressure drop

characteristics of the test section with the smooth tube friction data, a series of pressure drop measurements was made without heat input to the test section. Figure 12 shows a plot of the experimentally determined liquid friction factor versus Reynolds number. The solid line represents the smooth tube data available in the literature. A close agreement was observed between the smooth tube data and the experimental points, as shown, indicating that there was hydrodynamic smoothness.

C. Non-Adiabatic Pressure Drop

Several series of runs with different flow rates and heat flux values were made for non-adiabatic pressure drop measurements. Under non-adiabatic conditions, the pressure drop is the result of the frictional forces and of the rate of increase of momentum of the mixture. During all the pressure drop measurements, the thermocouple probes for the fluid temperature measurement were not placed in the test section. From these pressure drop measurements the pressure profiles along the test section were obtained.

Figure 13 shows typical pressure profiles for a series of runs made with constant flow rate, constant inlet temperature, and with different heat flux. On the same figure, curves representing the local bulk steam qualities also are given.

From the pressure profiles, the axial pressure gradients for two-phase flow, $(\frac{dP}{dl})_{TP}$, were calculated for each tap position along the boiling length of the test section. For comparing the pressure gradients obtained for different flow rates, the pressure gradients for the case of the adiabatic all-liquid flow at the

saturation condition were introduced. The ratio of the non-adiabatic pressure gradient to the adiabatic pressure gradient, $R = \frac{(dP/dl)TP}{(dP/dl)_o}$, was used in the presentation of the results.

This pressure gradient ratio was plotted as a function of a dimensionless parameter X which was first introduced by Martinelli and co-workers (4,14,15). The parameter X is defined as

$$X = \left(\frac{Vl}{Vg}\right)^{\frac{1}{2-n}} \left(\frac{\mu l}{\mu g}\right)^{\frac{n}{2-n}} \left(\frac{1}{x}-1\right) \tag{7}$$

Here n is the exponent of the Reynolds number in the friction factor equation. From the adiabatic pressure drop data n was found to be 0.25. Therefore,

$$X = \left(\frac{Vl}{Vg}\right)^{0.5n} \left(\frac{\mu l}{\mu g}\right)^{0.143} \left(\frac{1}{x}-1\right) \tag{8}$$

Figures 14, 15 and 16 show the plots of the pressure gradient ratio versus the parameter X for three different flow rates. For each flow rate several runs corresponding to different heat flux values are represented. A common feature is observed on these plots. That is, the curves corresponding to different heat flux values merge into a single curve below a certain X value. Also, this particular X value increases with an increase in the flow rate. Expressed from the standpoint of steam quality, which is the main variable in the parameter X, it may be said that above a certain quality the pressure gradient ratio, R, for a constant flow rate can be represented by a single curve and is independent of the heat flux. The quality corresponding to this merging point decreases as the flow rate is increased. For the cases illustrated, the merging points correspond to steam qualities of 20%, 10%, and 6% for

mass velocities of 1.38×10^5, 2.76×10^5 and 4.14×10^5 lb/hr ft^2 respectively. It is noted that an almost exact inverse ratio prevails between these corresponding X and G values. It is also observed that before merging, the curves corresponding to increasing heat flux, also corresponded to increasing pressure gradient ratios.

These observations and the study of the still and motion pictures of the outlet mixture led to the following postulates:

The merging of the pressure gradient ratio curves is the result of a change occurring in the flow and heat transfer mechanisms. Nucleat boiling and forced convection are two primary processes which control the heat transfer and the pressure drop characteristics of the system. For the low steam qualities and low mass flow rates nucleate boiling process seems to be dominant. Since for a constant flow rate a higher heat flux would correspond to a more vigorous boiling and a higher degree of turbulence, a higher pressure gradient ratio should be expected. In this region the flow pattern may be assumed to be more or less annular, composed of a steam core and of a liquid film on the walls which is thick enough to support bubble growth.

Above a certain range of the steam quality, the increased velocity of the two-phase mixture becomes sufficient to suppress the nucleate boiling process. In this region the liquid droplets are more or less homogeneously dispersed in the high-velocity steam phase. And the system characteristics are governed by the forced convective process. This flow pattern corresponds to what has been termed in the literature as fog, homogeneous or liquid-dispersed flow. Although the actual flow pattern is not yet clearly defined, it is generally thought that a very

rapid exchange of liquid droplets between the walls and the main stream is responsible for the transfer of heat. In a recent paper, Goldmann and co-workers (16) proposed that the liquid transport to the walls is accomplished by eddy diffusion of droplets.

This change in the flow mechanism and the accompanying disappearance of the liquid film and of the nucleate boiling on the walls is suggested as the explanation of the observed merging of different heat flux curves in Figures 14, 15 and 16.

As a result of the foregoing, the region in which the pressure gradient ratio curves are separated might be called "nucleate boiling region" and the region corresponding to the merging of these curves might be called "liquid-dispersed region". Similar conclusions and the distinction between heat transfer mechanisms were forwarded by some previous workers (6,11) from the standpoint of the local heat transfer coefficients in non-adiabatic two-phase flow systems.

The following comparison is made as a further remark in connection with the merging points of the pressure gradient ratio curves, which are interpreted as the transition points toward a liquid-dispersed flow pattern.

Figure 17 showing a flow pattern chart for a steam-water system at atmospheric pressure is taken from the reference (16). For the sake of clarity only the curves corresponding to the atmospheric pressure are reproduced from the original chart which also included similar curves for 800 psia and 1500 psia pressures. The mass velocities and the steam qualities at the merging points corresponding to Figures 14, 15 and 16 are marked on this chart. Even not considering the fact that

the boundaries between flow patterns shown as lines in the chart are in reality diffuse bands, the favorable comparison is interesting.

The liquid-dispersed region pressure gradient ratio curves of Figures 14, 15, and 16 are compared with each other in Figure 18. A slight effect of the mass velocity on the ratio R is noticed. The ratio R increases with increase in mass velocity for the same X value. Within the range of mass velocities studied, this effect can be expressed as,

$$R \sim [G]^{0.25} \tag{9}$$

Consequently a correction in this form was applied to the curves in Figure 18. Figure 19 shows that when plotted as $R[10^{-5}G]^{-0.25}$ versus X the liquid dispersed region data can be represented by a single curve for all the flow rate and heat flux range studied.

Since the main variable in the parameter X was the steam quality, x, a plot of the ratio R versus x in the liquid dispersed region also was tried. Here again a slight mass velocity effect was observed. With a resulting correction Figure 20 shows a plot of the $R[10^{-5}G]^{-0.1}$ values versus x. It is seen that all the data may be represented, within $\pm 15\%$, by the expression

$$R[10^{-5}G]^{-0.1} = 0.437 \times 10^{4} X^{1.32} \tag{10}$$

D. Comparison of the Non-Adiabatic Pressure Drop Results with that of Previous Workers

a) Reference (8) reports an investigation on the forced circulation boiling of water in an electrically heated horizontal tube at operating pressures of 30-200 psia. The following empirical correlation was presented for the variation of the pressure gradient ratio as a function

of mass fraction evaporated and absolute system pressure,

$$R = \frac{0.795 \times 10^5 \, x^{1.93-0.37 \log P}}{P^{1.04}} + 6 \qquad (11)$$

Here R was obtained by averaging the values corresponding to different flow rates. Although the lowest system pressure studied was 30 psia, this relationship would be reduced to the following form, for the case of $P = 14.7$ psia,

$$R = 0.485 \times 10^4 \, x^{1.50} + 6 \qquad (12)$$

It is of similar form with the expression (10) given above as representing the liquid-dispersed region data of the present work. In Reference (8) the Equation (11) was presented to cover all the experimental data. However it should be pointed out that, since the mass velocity range studied was 3.9×10^5 to 12.9×10^5 lb/hr ft^2, the liquid-dispersed region was probably reached for much smaller qualities than in the present work and most of the data belonged to this region. In this respect it is interesting to note the author's remark that higher pressure gradient values were obtained during a few runs made with shorter boiling lengths and consequently with lower exit qualities.

b) Martinelli and Nelson[15] proposed a method for the calculation of pressure drop during forced-circulation boiling of water in horizontal tubes. The method was an extension to steam-water mixtures of the correlations based mostly upon the isothermal two-phase two-component data.

The over-all pressure drop measurements of the present work have been compared with the pressure drop values predicted by this method. For

this purpose, some of the original curves given in Reference (15) were re-plotted in a manner to permit more accurate readings for the pressure and quality values studied. In order to obtain a greater number of points for this comparison, the pressure drop between the incipient boiling point and each pressure tap was taken as corresponding to an independent run. The pressure value used in the calculations was taken equal to the average of the measured pressures in that part of the test section used in the comparison.

Figure 21 shows this comparison. It is seen that in all cases, the measured pressure drop values fall within the values predicted for separated and fog flow models. For a small pressure drop (low flow rates and low qualities), the separated flow predictions are in better agreement with the measured values, while the fog flow predictions largely overestimate the pressure drop. As the pressure drop increases a trend is observed toward an improved agreement between the fog flow predictions and the measured values.

Another comparison between the measured and predicted pressure drop is shown in Figure 22. In this figure, the measured pressure drop between the incipient boiling point and the successive pressure taps along the test section for a particular run is shown together with the predicted curves corresponding to fog flow and separated flow. A curve representing the calculated local steam qualities also is included. It is seen that with increasing quality the measured pressure drop characteristic follows a transitional form from that of a separated flow mechanism to that represented by a fog flow mechanism. Similar plots were repeated for each run

and on all these plots the same tendency of the measured pressure drop curve was observed.

This observation led to the concept of correlating the actual pressure drop curve using a linear combination of the separated and fog flow pressure drop characteristics in the following manner:

$$\Delta P_{ACT} = m \cdot \Delta P_{SEP} + n \Delta P_{FOG} \tag{14}$$

In which it is assumed that

$$m + n = 1 \tag{15}$$

since this is the trend at the limits of large and small qualities. From these two equations,

$$m = \frac{\Delta P_{FOG} - \Delta P_{ACT}}{\Delta P_{FOG} - \Delta P_{SEP}} \tag{16}$$

$$n = \frac{\Delta P_{ACT} - \Delta P_{SEP}}{\Delta P_{FOG} - \Delta P_{SEP}} \tag{17}$$

Consequently m and n values were calculated for several runs and plotted versus steam quality. Figure 23 shows the plot of the coefficient m for three different mass velocities. The points belonging to each mass velocity could be represented by a separate curve. Then it was tried to combine these three separate curves into a single curve by a change of the co-ordinates. Figure 24 is the result of such a modification, and the m values for all the mass velocities were grouped together and represented by a single curve within a certain scatter of data, when plotted versus the product $10^{-4}\ x^{1.47}\ G$.

E. Wall Temperatures

For measuring the outside tube wall temperatures, twenty thermocouples were placed at the top and bottom of the test section at several

stations. During the preliminary measurements some differences and changes had been observed between the top and bottom temperatures under certain conditions. And for a better interpretation of the temperature measurements, a test section which would have no pressure taps or thermocouple probe attachments seemed to be more desirable from the standpoint of the heat generation uniformity. Consequently, such a test section of the same general dimensions as the original one was built using the same tubing material. And the wall temperature measurements were carried out on this test section. The location of the wall thermocouples are indicated in the Figures 25, 26, and 27.

The temperature drop across the tube wall was calculated using the Equation (6), for determining the inside wall temperatures. The data of Dickinson and Welch[17] was used for the thermal conductivity of AISI type 304 stainless steel.

Figures 25, 26, and 27 show the inner wall temperatures for three series of runs made with different mass velocities, constant inlet temperature and increasing heat flux. The exit qualities corresponding to each run also are specified.

If Figure 25 which belongs to the lowest mass velocity, the first run is an adiabatic run with water at 205°F. The purpose of this run was to check the uniformity of the thermocouple readings. In the two following runs corresponding to exit qualities of 2% and 5%, the upper wall temperatures were found to be consistently lower than the lower wall temperatures. The difference was about 10-12 °F. The photographic study of the outlet mixture showed an unsteady, pulsating, stratified flow pattern for these conditions (see Figures 28, 29, 30, 31, 32). Lower

temperatures observed at the upper portion of the test section are attributed to a more effective transfer of heat between the upper wall and the high-velocity steam phase (including the entrained water) which is moving in the upper portion of the tube cross-section.

As the heat flux is further increased during the following runs, it is observed that the difference between the upper and lower wall temperatures disappears, and for most of the locations both temperatures become essentially the same. This is in agreement with the observed more symmetrical flow patterns as the heat flux increases. (Figure 35-39).

The same general remarks can be made about Figure 26. However, in the first two runs with low heat flux the temperature difference between upper and lower portions was smaller than in the first series of runs.

During the runs made with the highest mass velocity studied and shown in Figure 27, no similar temperature difference between the upper and lower portions of the tube wall was found.

F. Photographic Study of the Outlet Mixture

Since the outlet of the test section was open to the atmosphere a photographic study of the outcoming steam-water mixture was conducted. Still pictures were taken with a 4 in. x 5 in. Speedgraphic camera which was used with a strobelight unit of 0.5 millisecond duration. Super panchro press type film was used with an F18 aperture. Motion pictures were also taken with a medium speed Fast-Air 16mm camera at a speed of 300 frames/second, using tri-x negative film.

Some of the still pictures are shown in Figures 28-39.

Figures 28, 29, 30, 31, and 32 were taken under the same experimental conditions which were $G = 1.38 \times 10^5$ lb/hr ft^2, $t_{in} = 205°F$, $q/A = 25000$ BTU/hr ft^2, $x_e = 5.5\%$. As seen by the pictures, the flow was unsteady, and consisted mainly in a pulsating stratified flow with alternate slugs of liquid and vapor.

Figures 33-34 correspond to a similar flow condition with a different mass velocity.

Figures 35, 36, and 37 correspond to annular flow patterns. Essentially this pattern consists of a core of vapor which may contain some water in the form of droplets, and of a liquid film on the tube walls.

Figures 38 and 39 are typical photographs corresponding to high steam qualities and to a liquid-dispersed flow pattern. The mixture is in the form of a more or less homogeneous dispersion of water droplets in the steam phase.

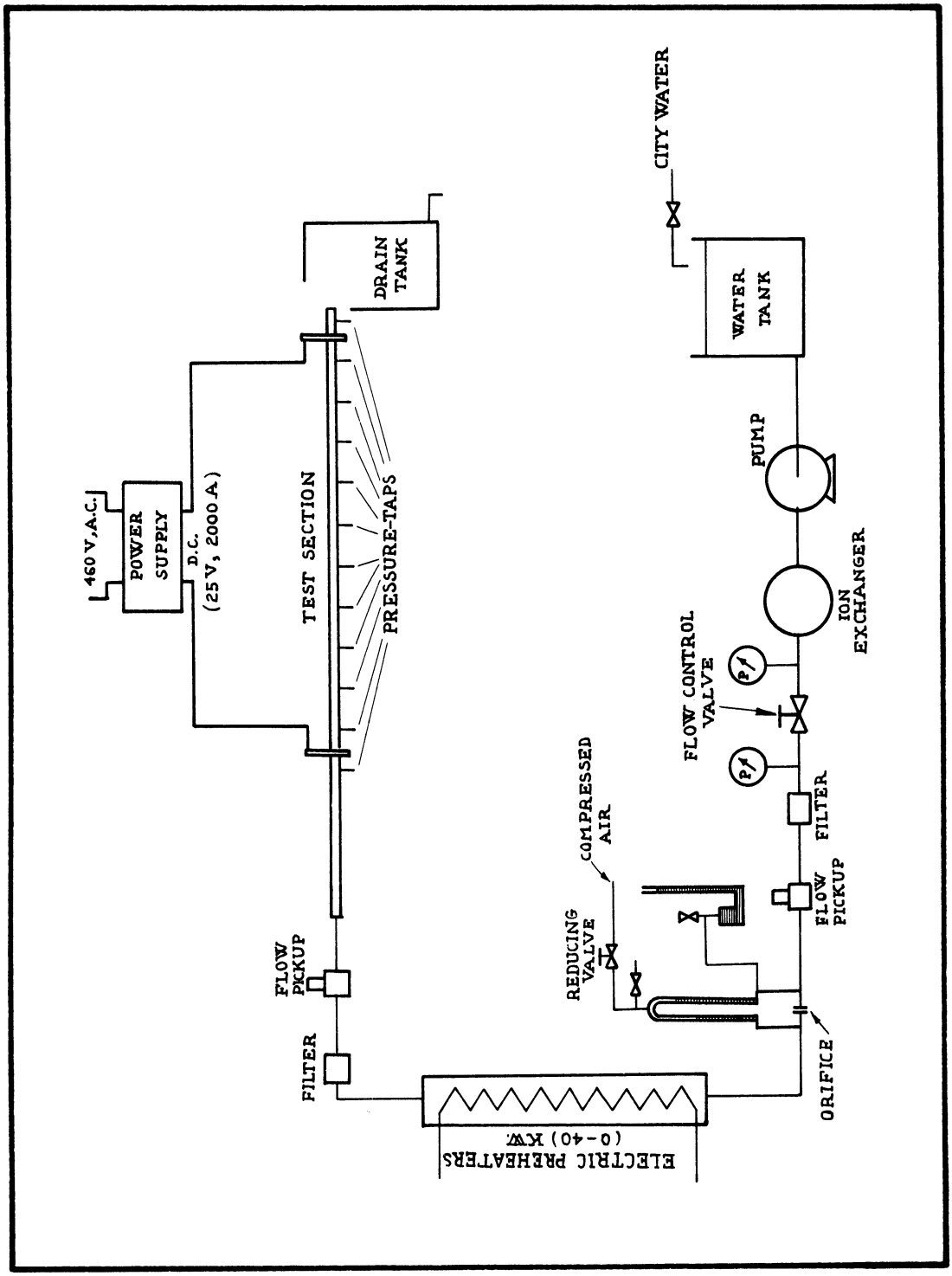

Figure 1. Schematic Diagram of the Equipment.

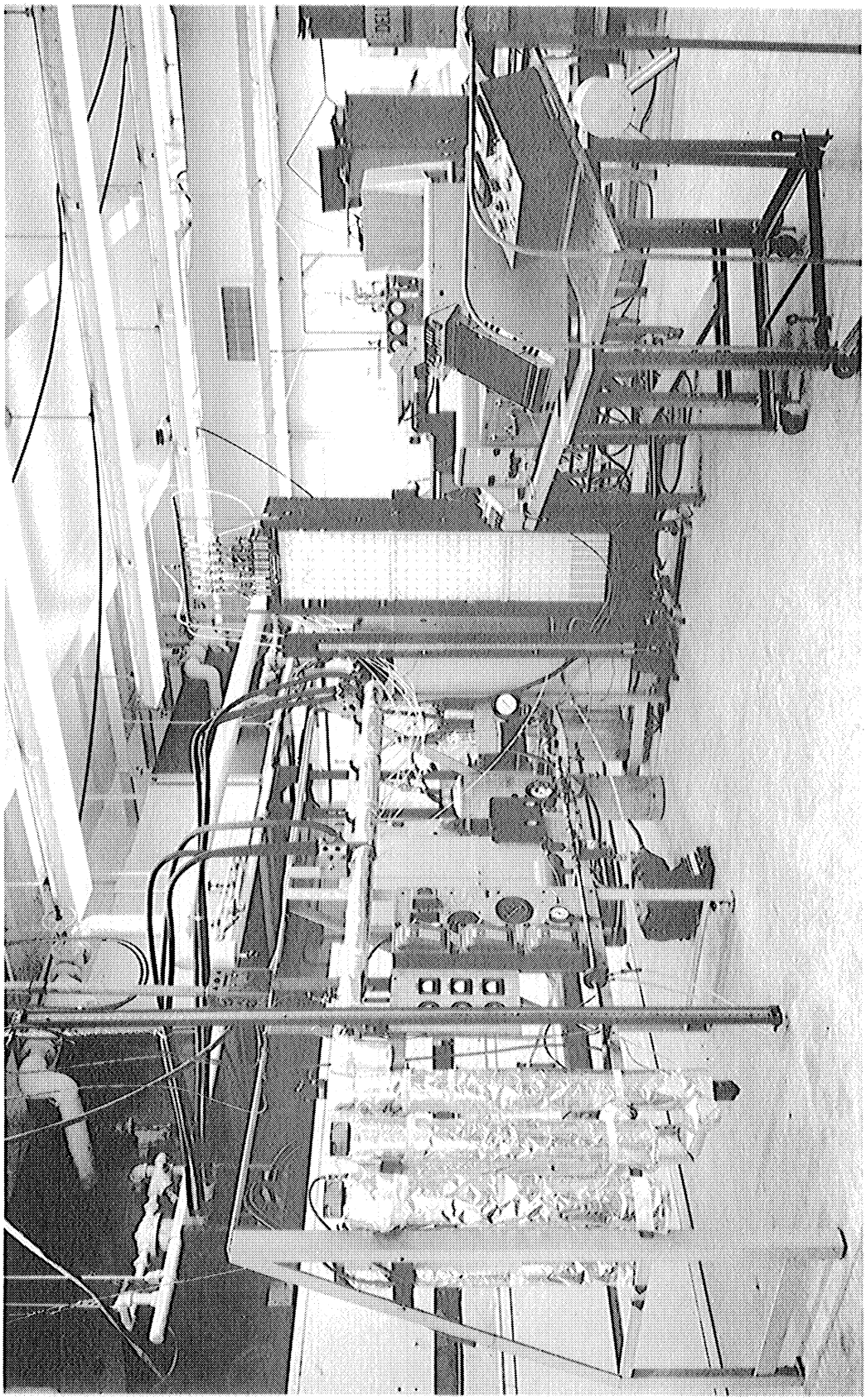

Figure 2. Over-all View of the Equipment.

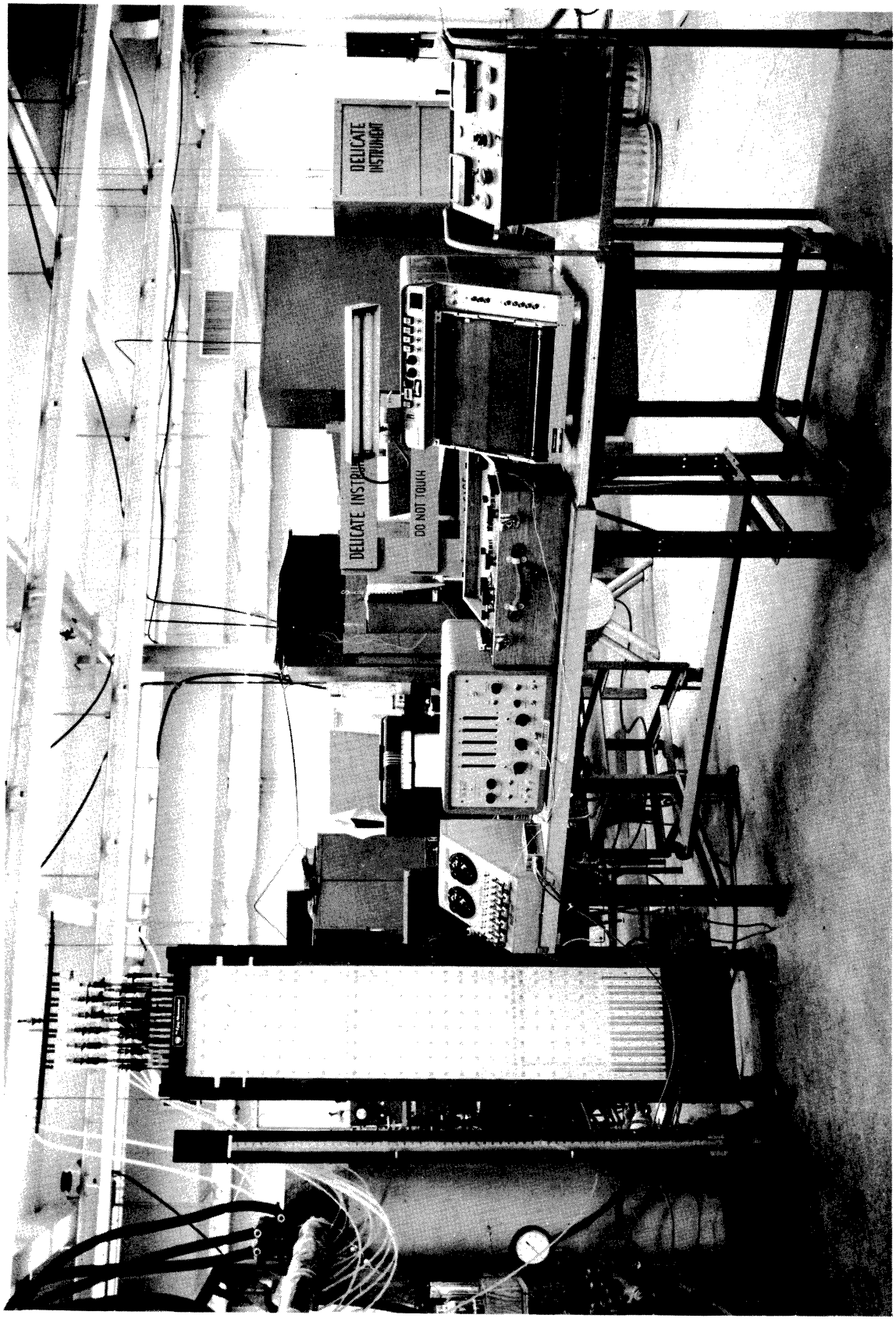

Figure 3. Close-up of the Instruments.

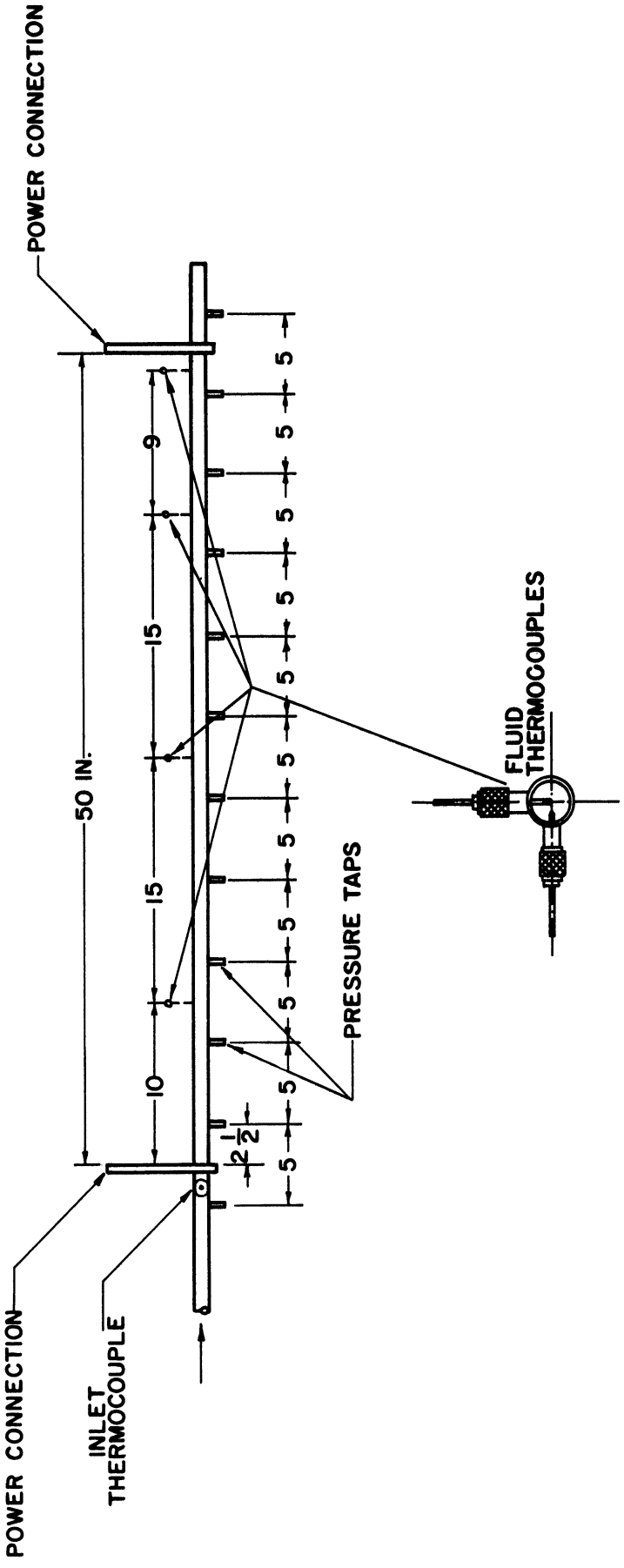

Figure 4. Detail of the Test Section.

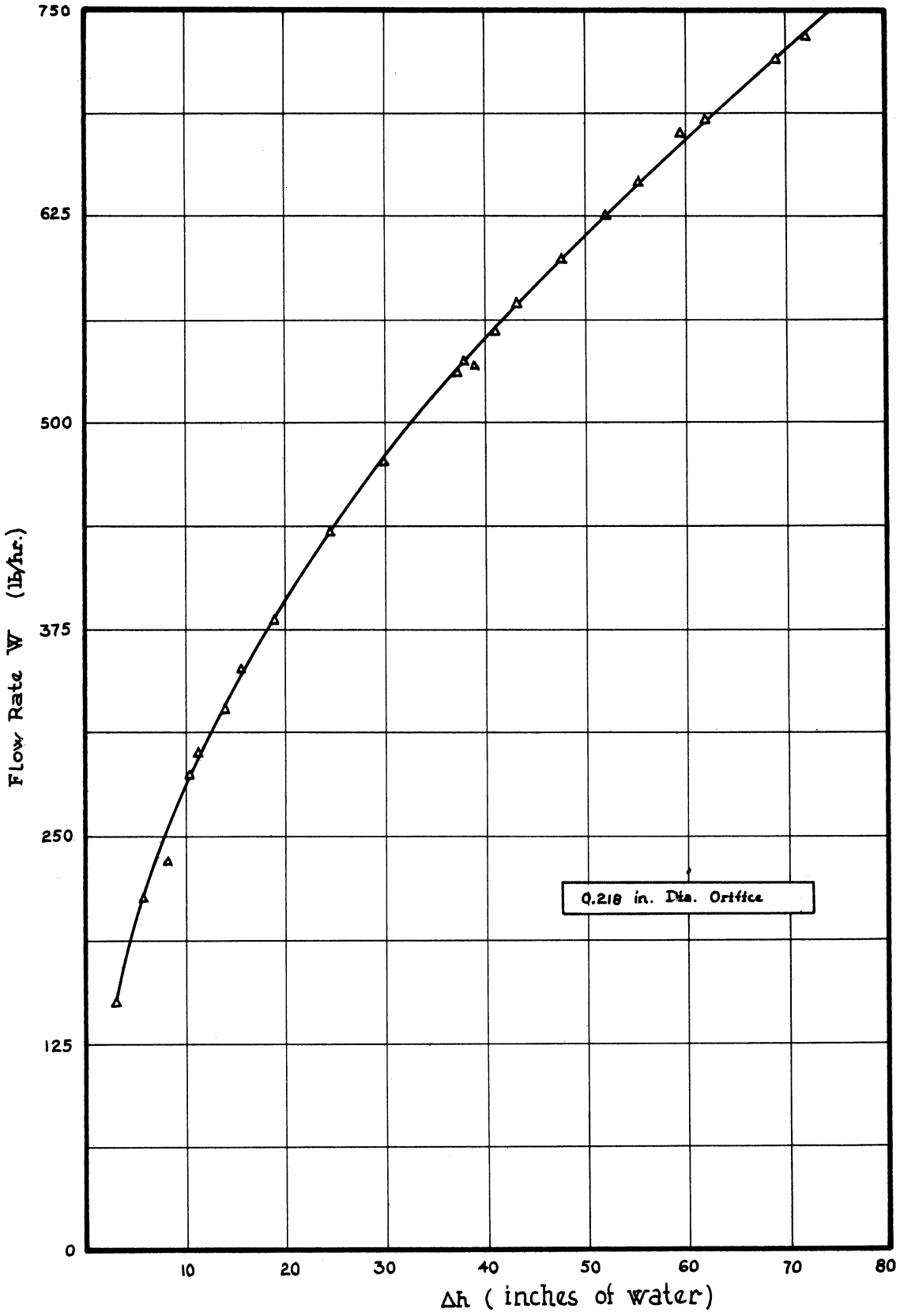

Figure 5. Calibration Curve for the 0.218 in. Diameter Orifice

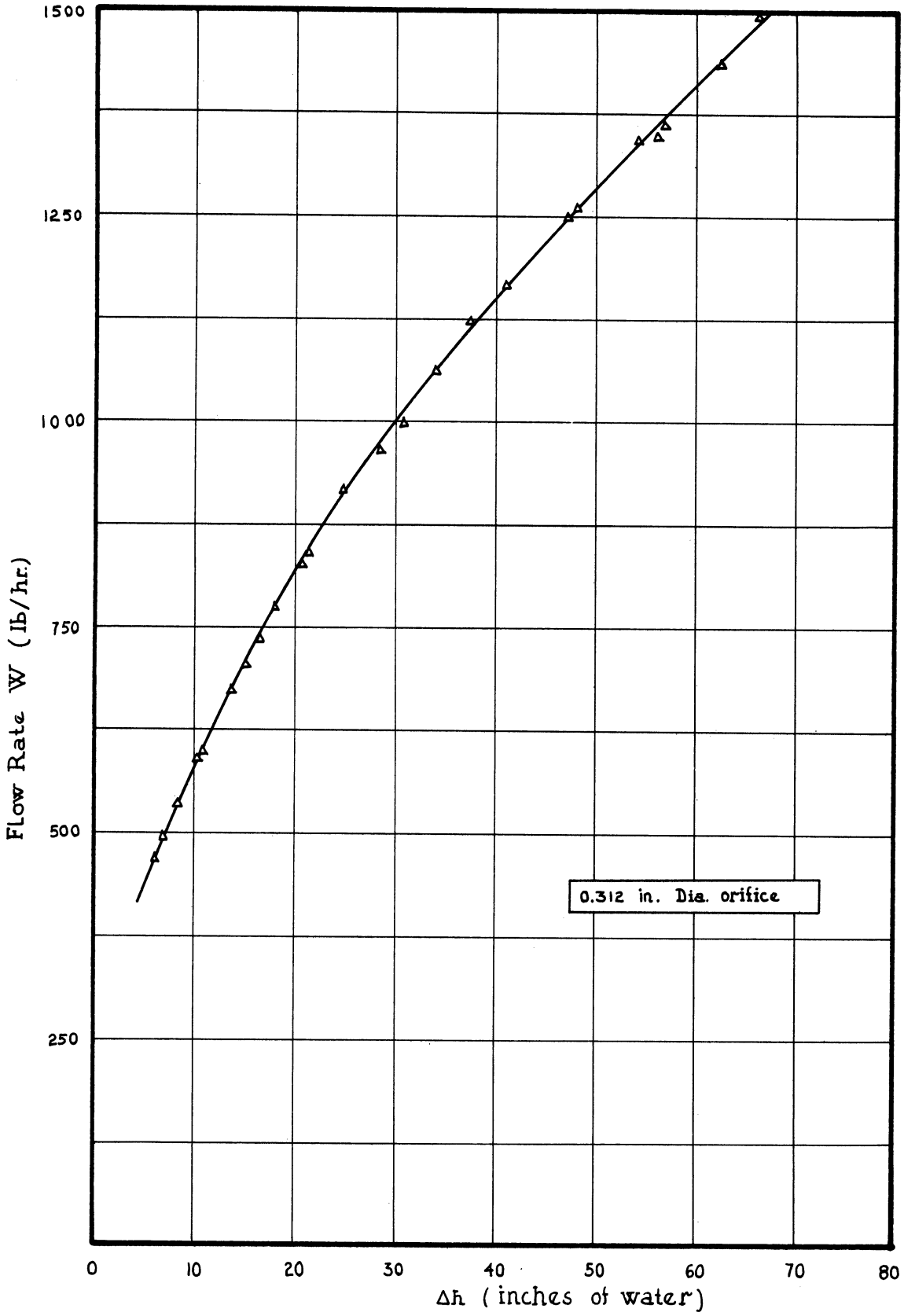

Figure 6. Calibration Curve for the 0.312 in Diameter Orifice.

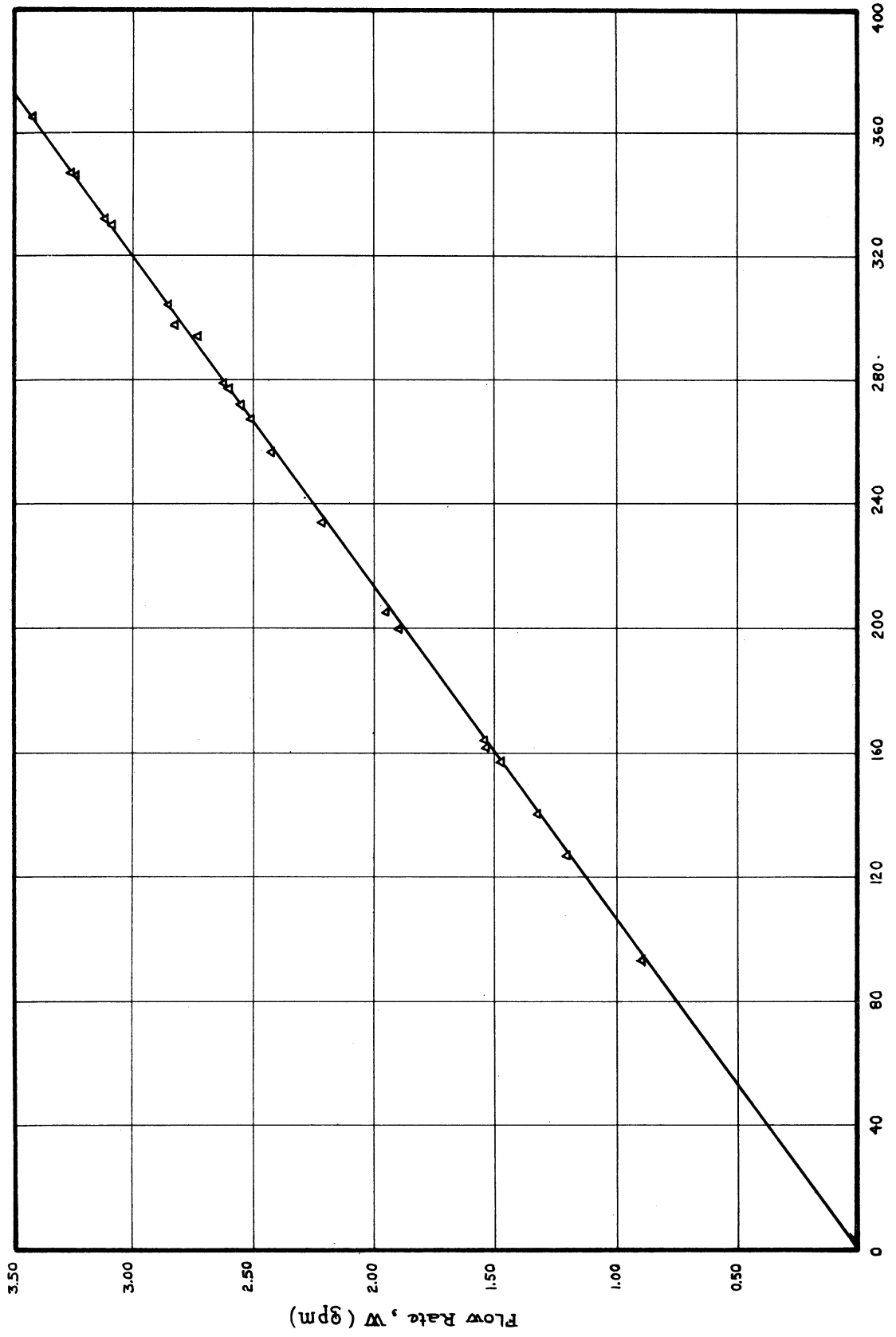

Figure 7. Calibration Curve for the Turbine Type Flowmeter.

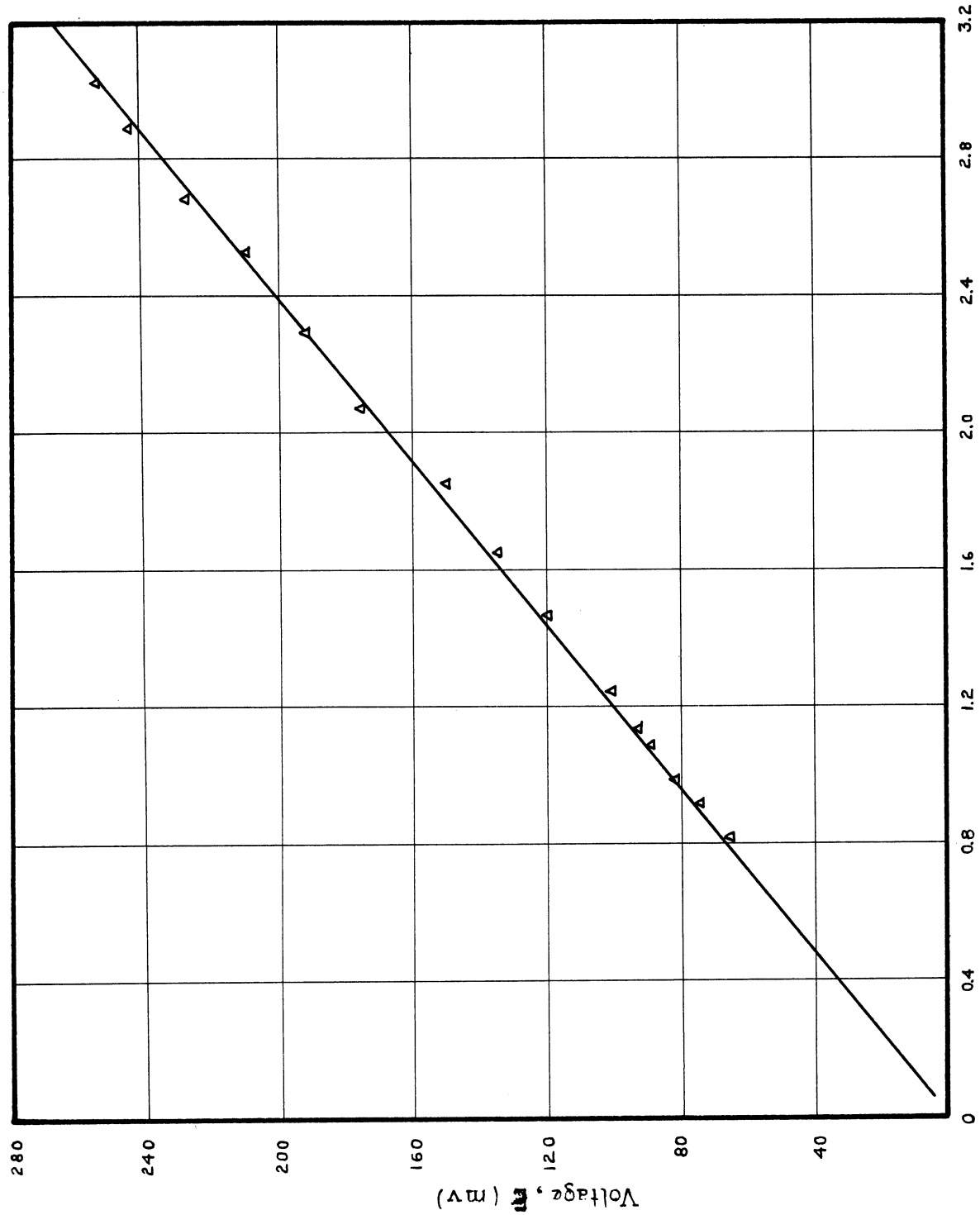

Figure 8. Flowmeter Output Voltage (Peak-to-Peak) versus Flow rate.

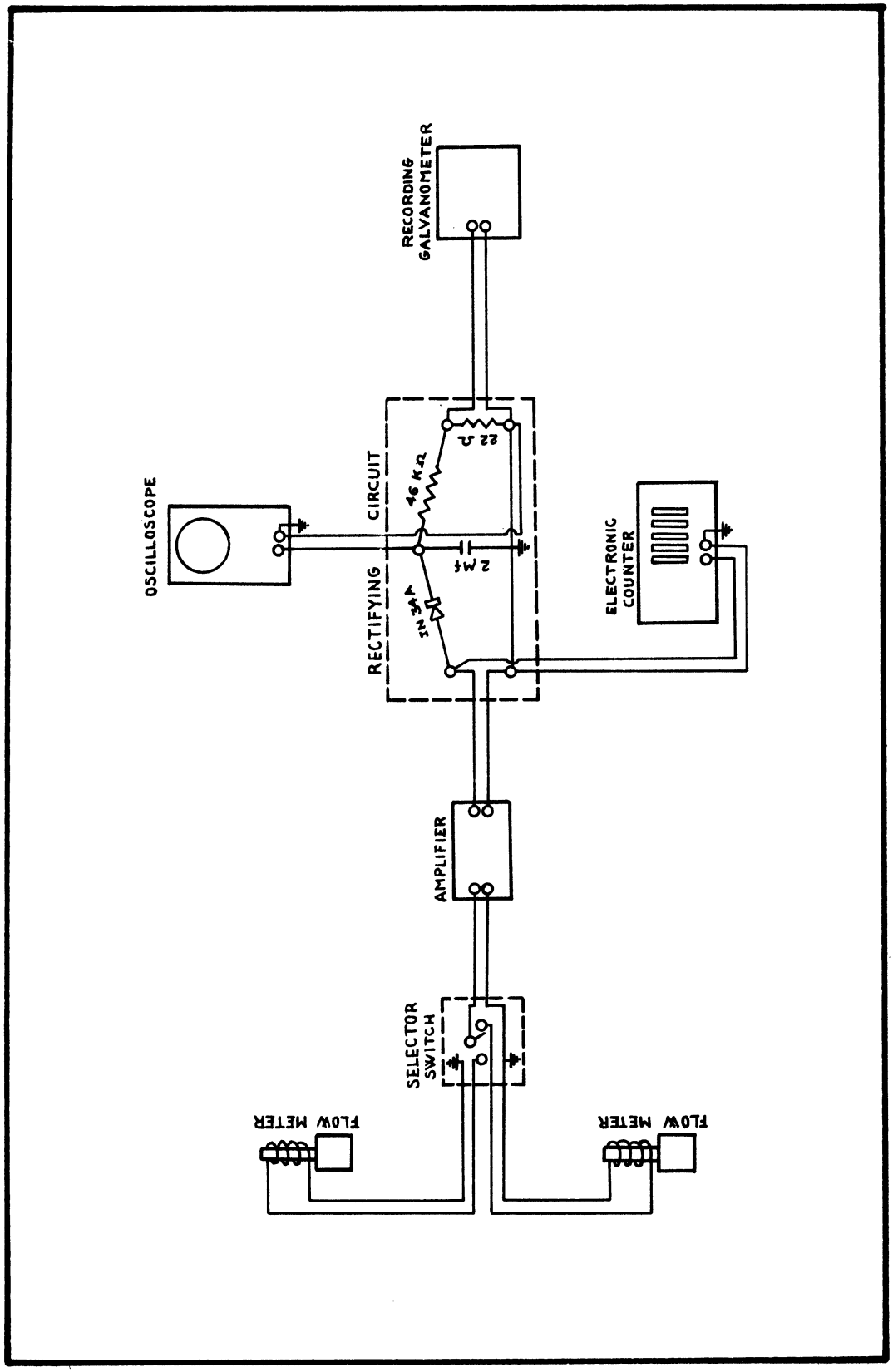

Figure 9. Electrical Circuit for the Measurement and Recording of the Flow Rate by Means of the Flowmeter.

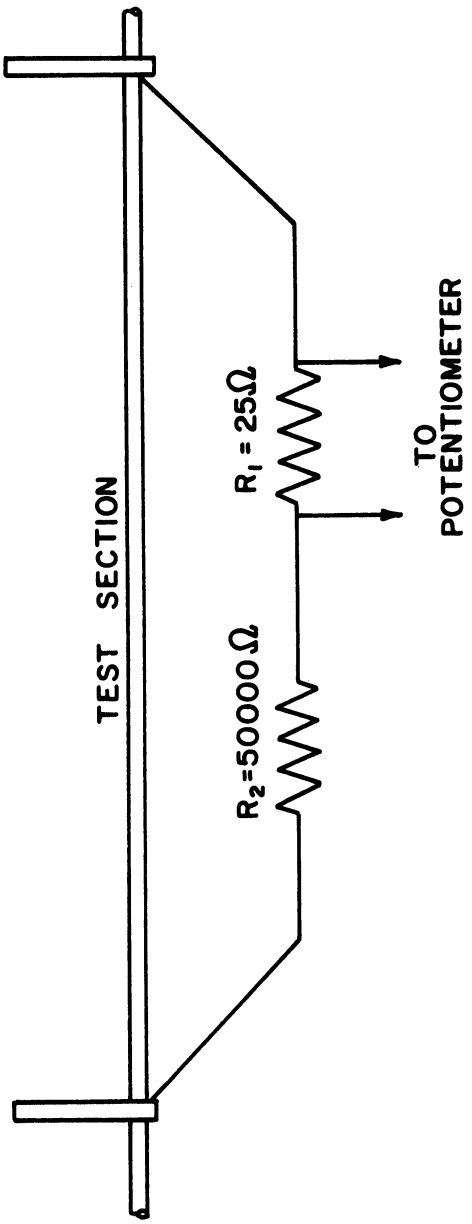

Figure 10. Voltage-divider Network for the Test Section Voltage Drop Measurement.

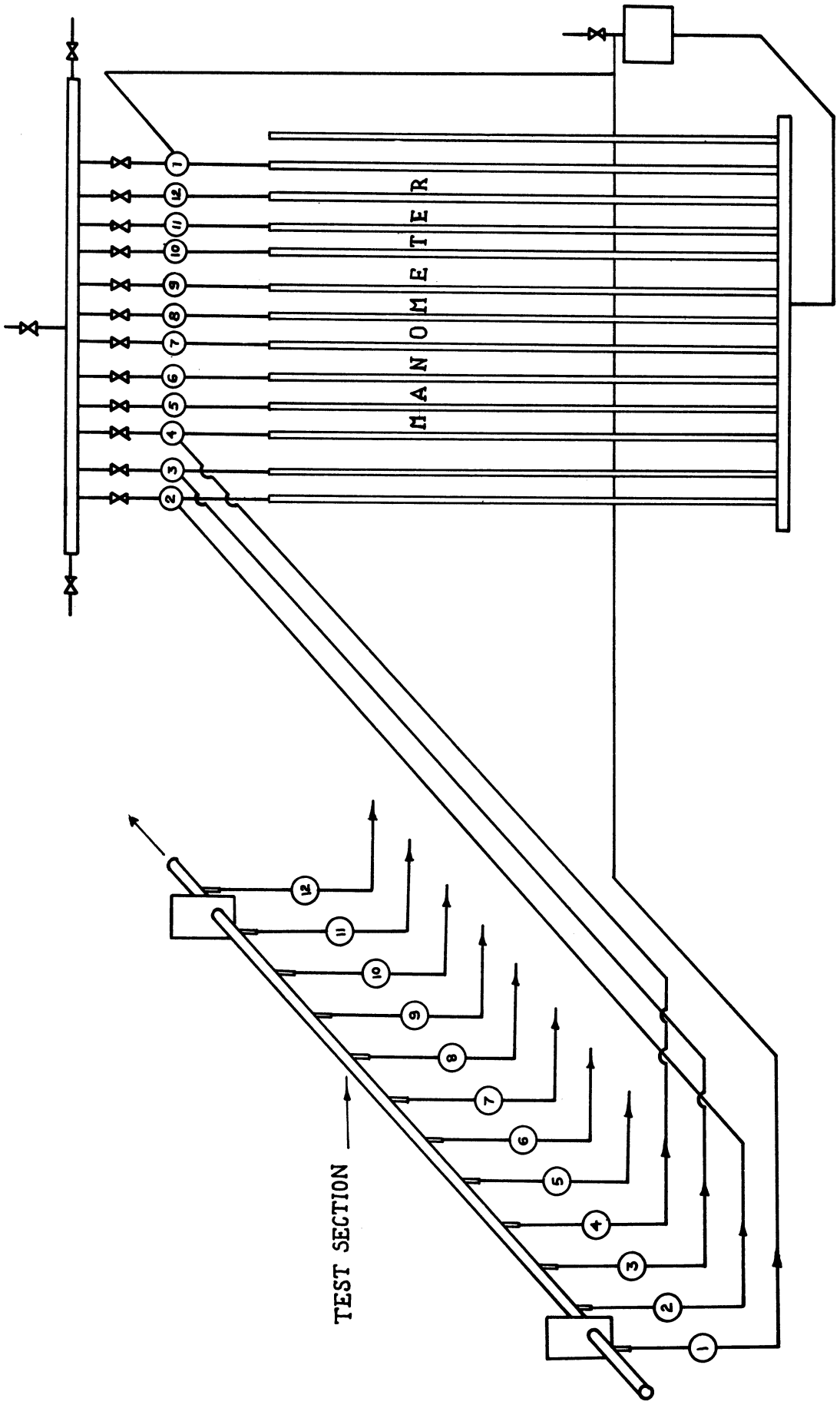

Figure 11. The Pressure Tap and Manometer Connections.

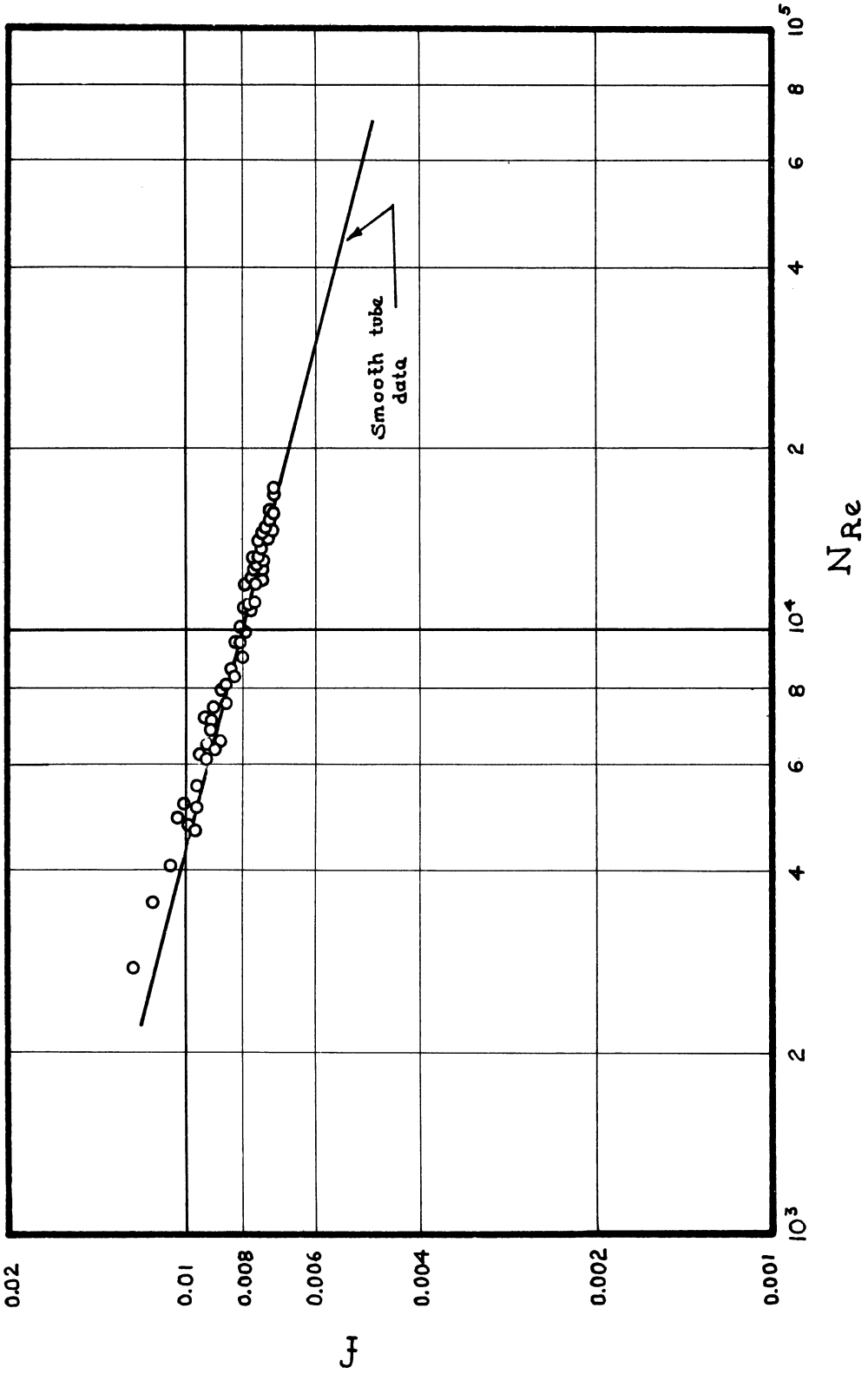

Figure 12. Friction Factor versus Reynolds Number for Adiabatic Runs.

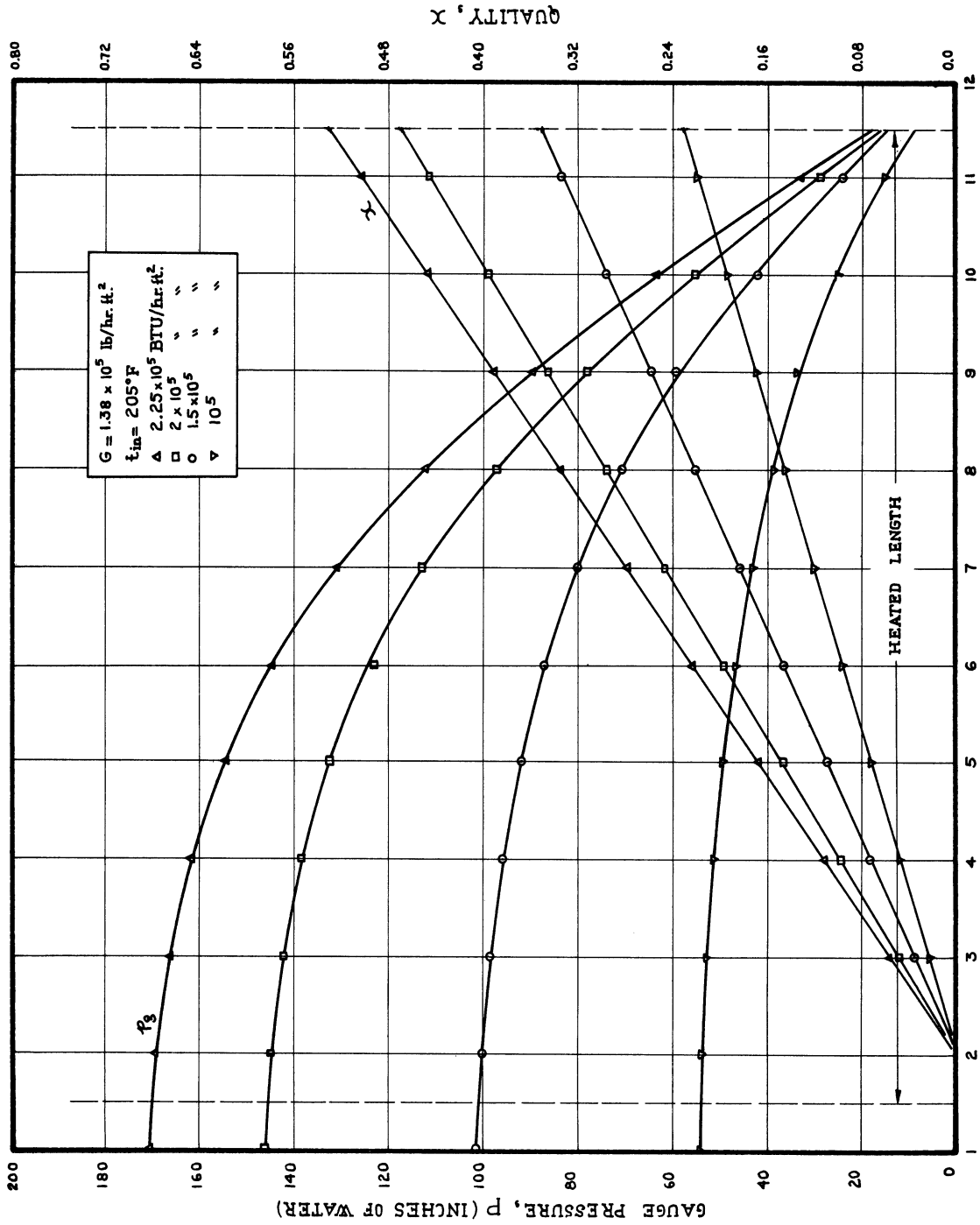

Figure 13 Pressure Profiles and Steam Quality Curves for a Series of Non-Adiabatic Runs.

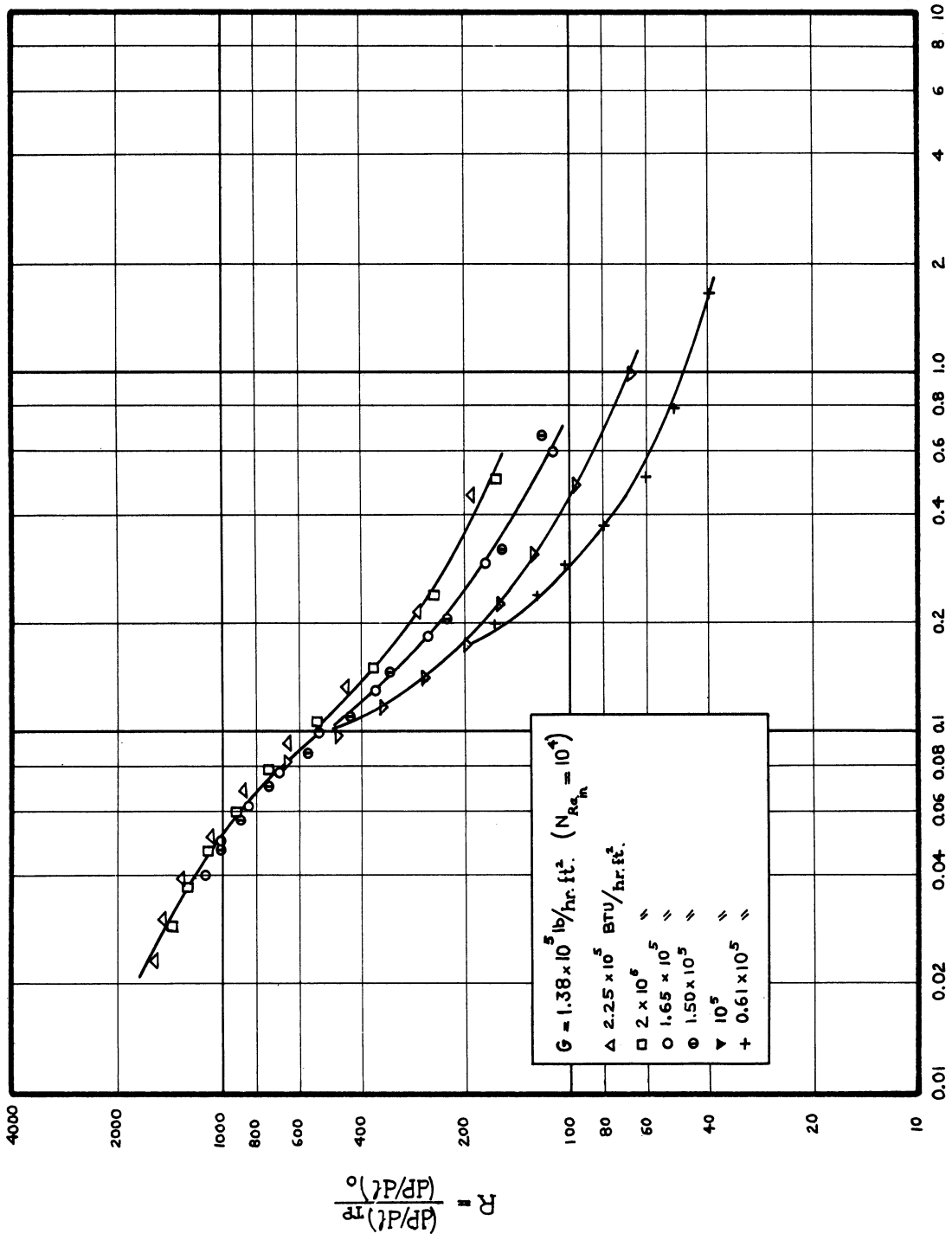

Figure 14. Plot of R versus X for G = 1.38 x 10^5 lb/hr ft^2

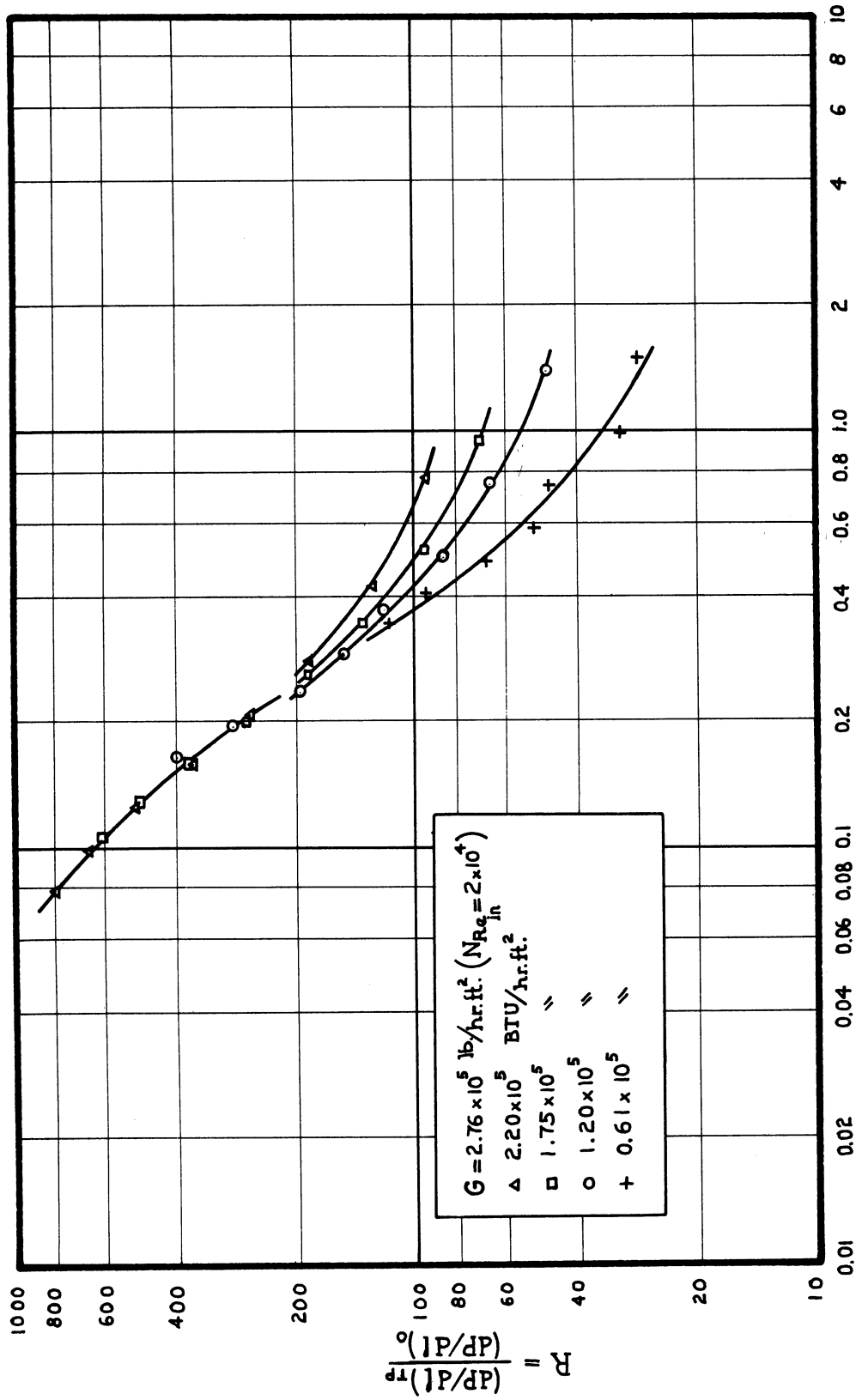

Figure 15. Plot of R versus χ for G = 2.76×10^5 lb/hr ft^2

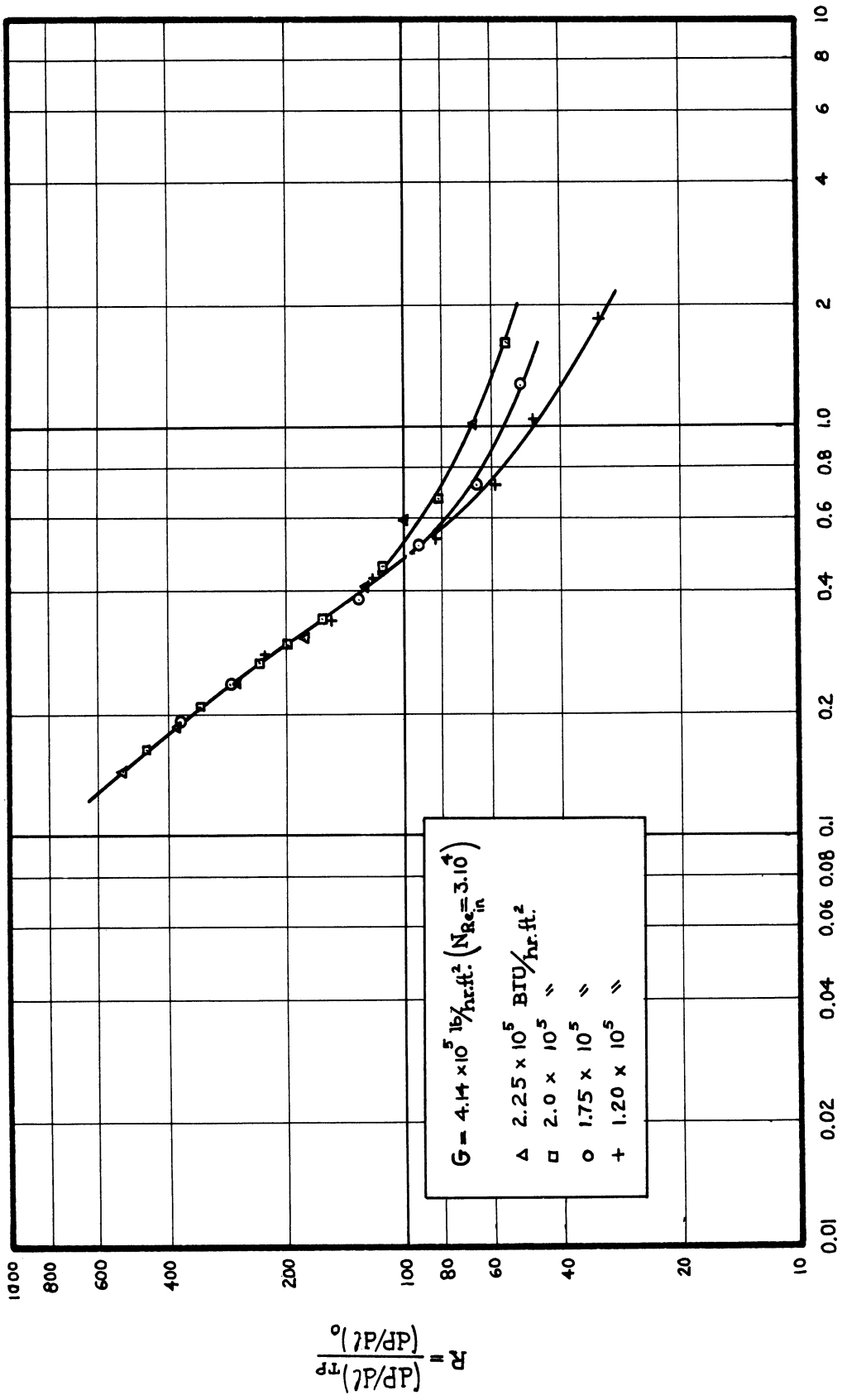

Figure 16. Plot of R versus χ for G = 4.14 x 10^5 lb/hr ft^2.

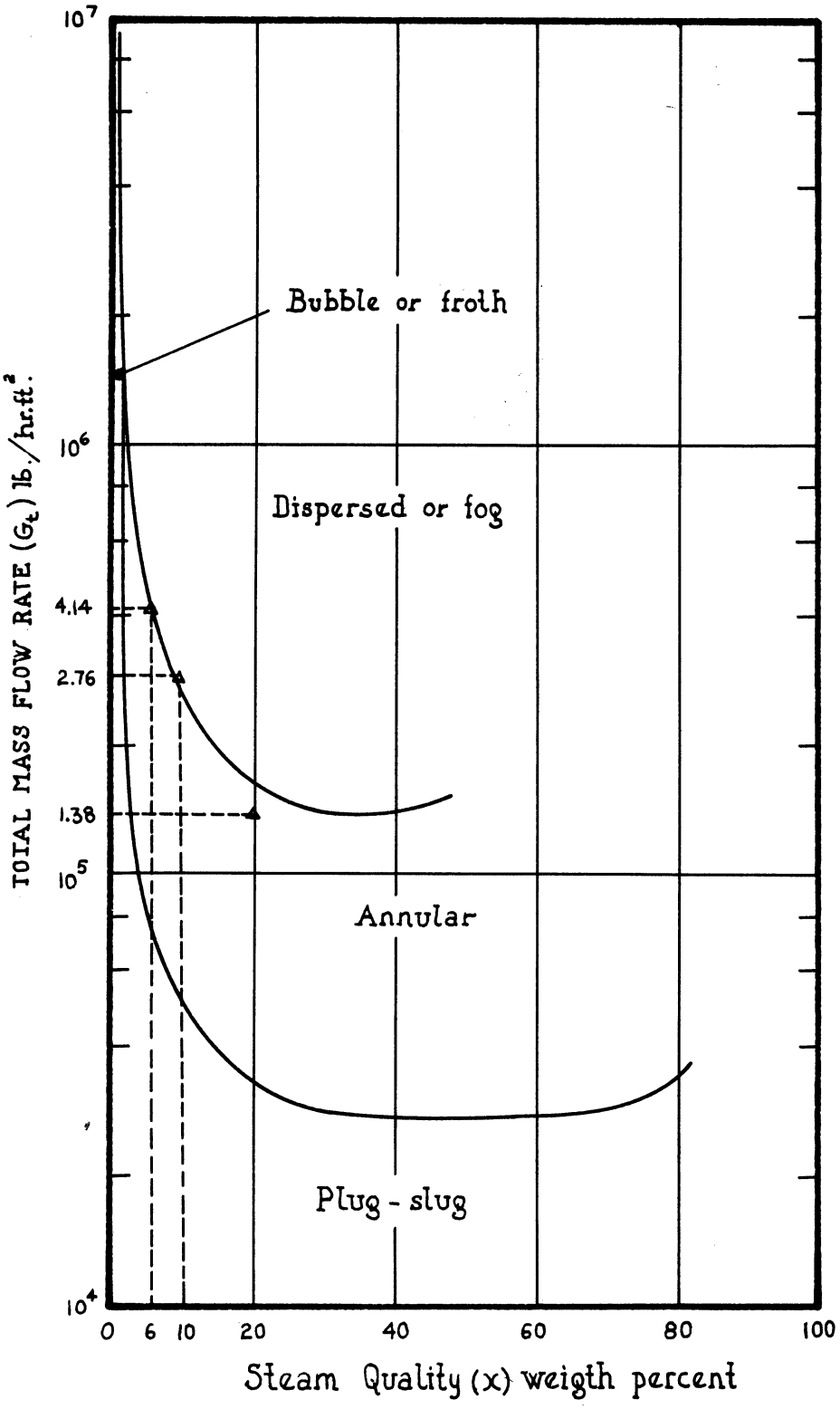

Figure 17. Comparison of the Experimental Results with the Steam-Water System Flow Pattern Chart for 14.7 psia (chart taken from reference 16).

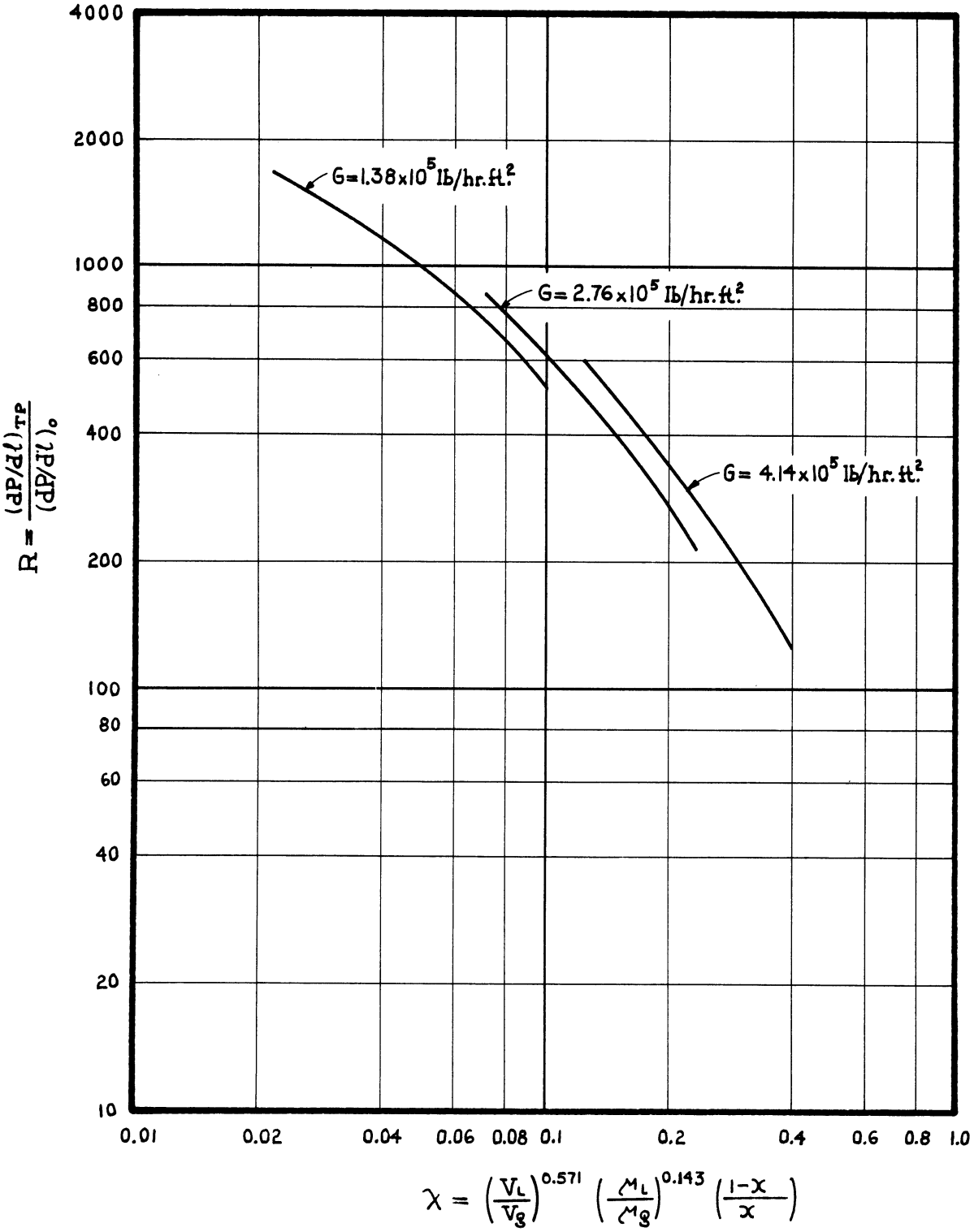

Figure 18. Comparison of the R-X curves in the Liquid-Dispersed Region.

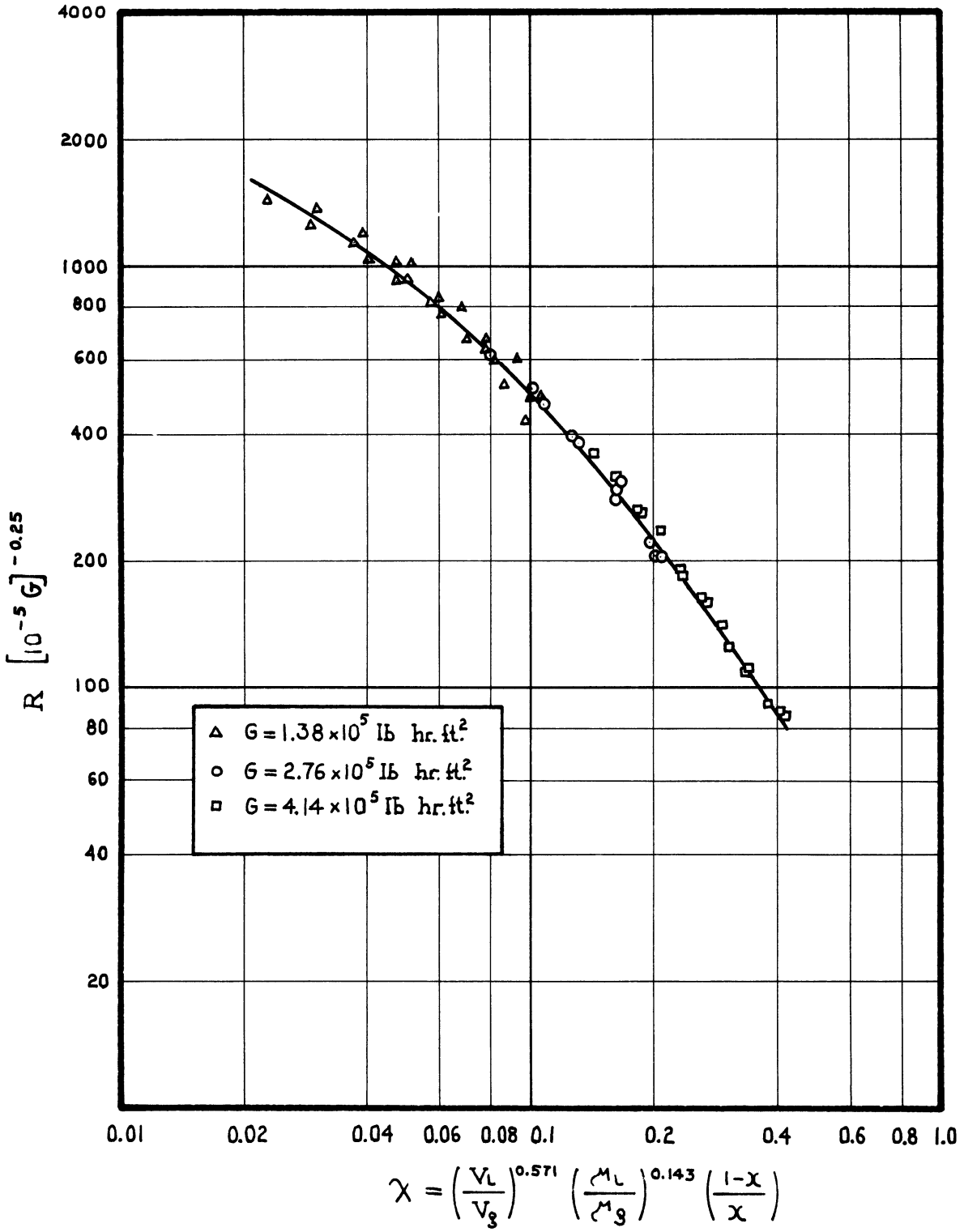

Figure 19. Plot of $R[10^{-5}G]^{-0.25}$ versus X in the Liquid-Dispersed Region

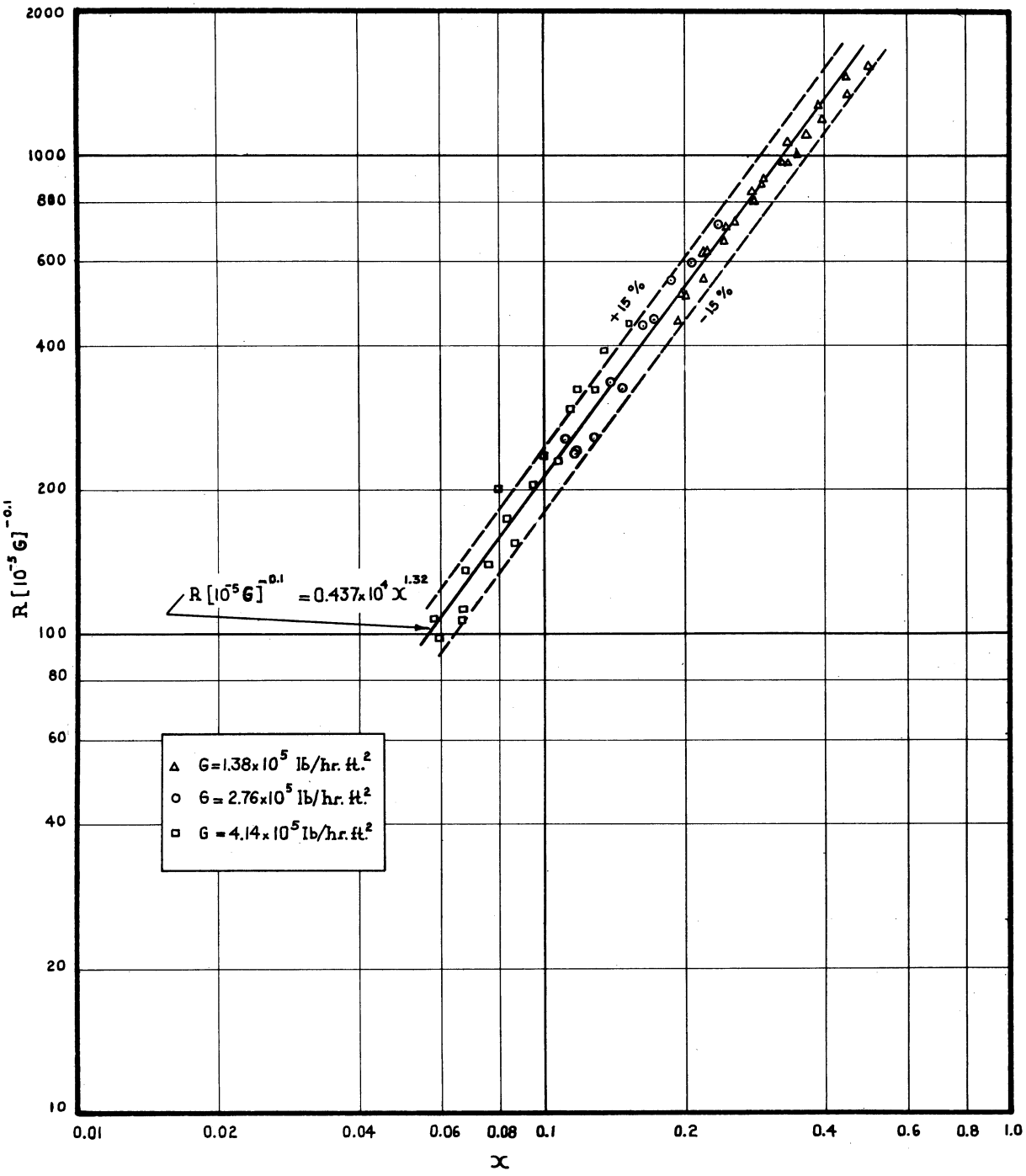

Figure 20. Plot of $R[10^{-5}G]^{-0.1}$ versus X in the Liquid-Dispersed Region.

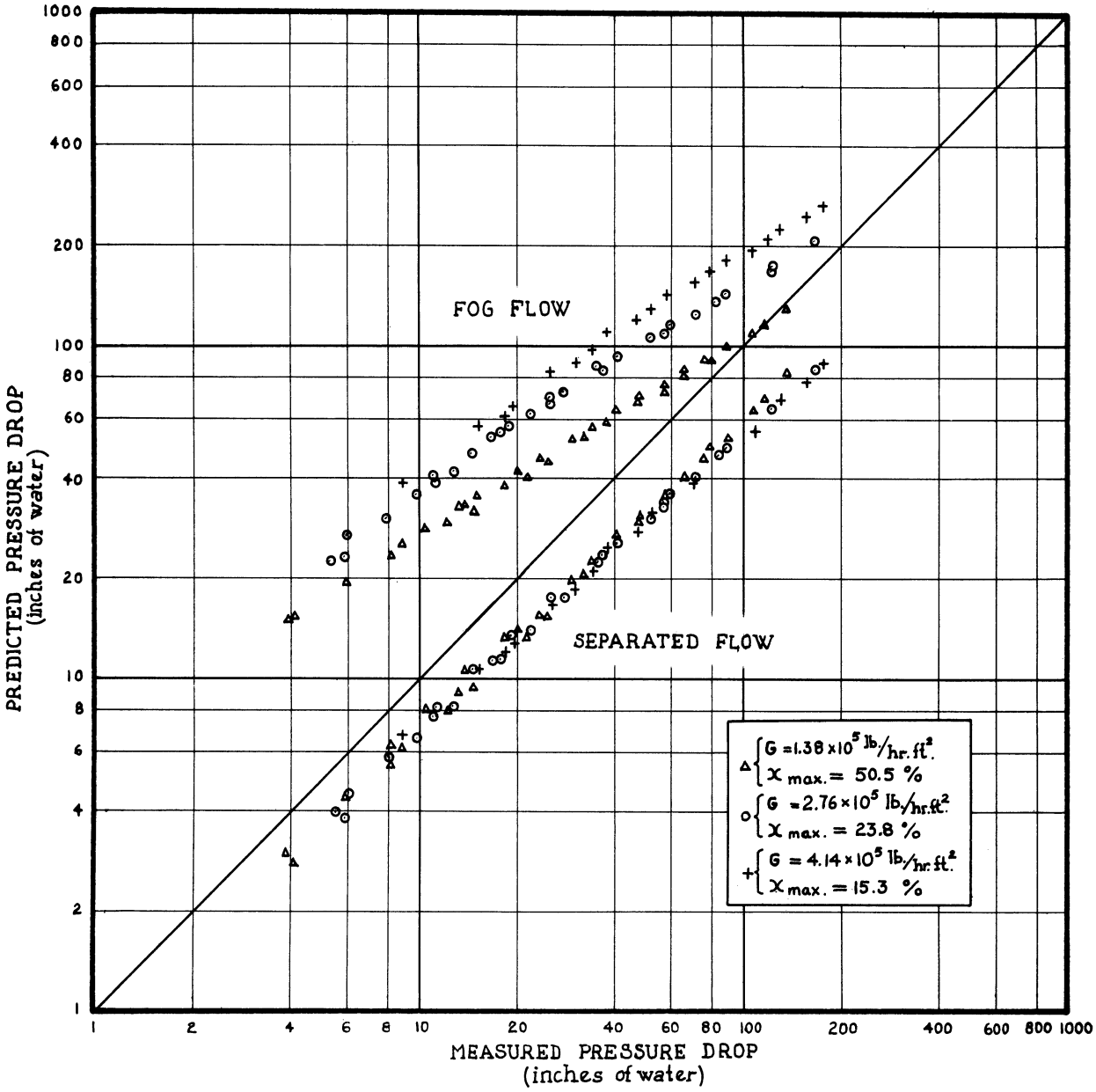

Figure 21. Comparison of the Measured Pressure Drop with the Predictions of the Martinelli-Nelson Correlation.

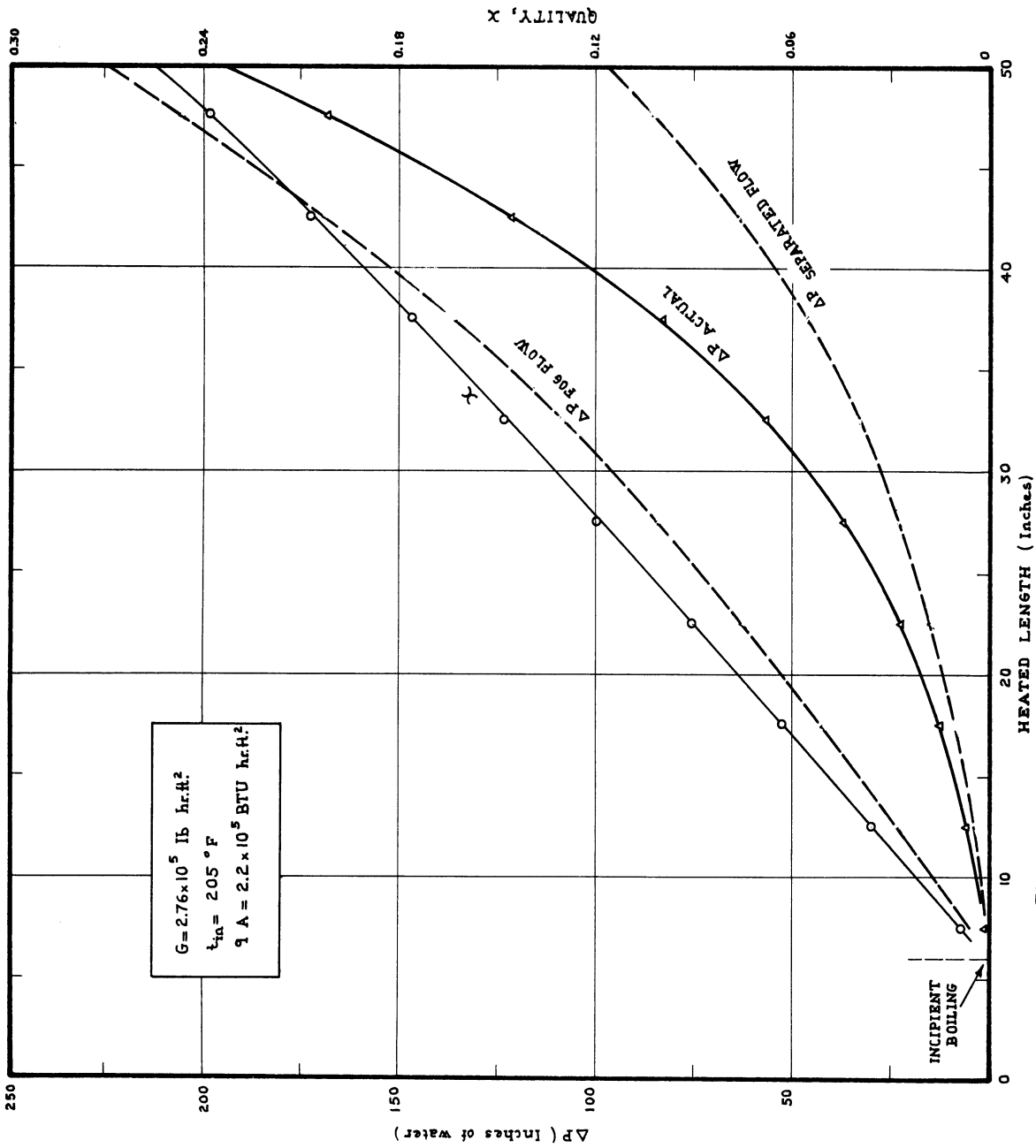

Figure 22. Comparison of the Measured and Predicted Pressure Drops along the Test Section.

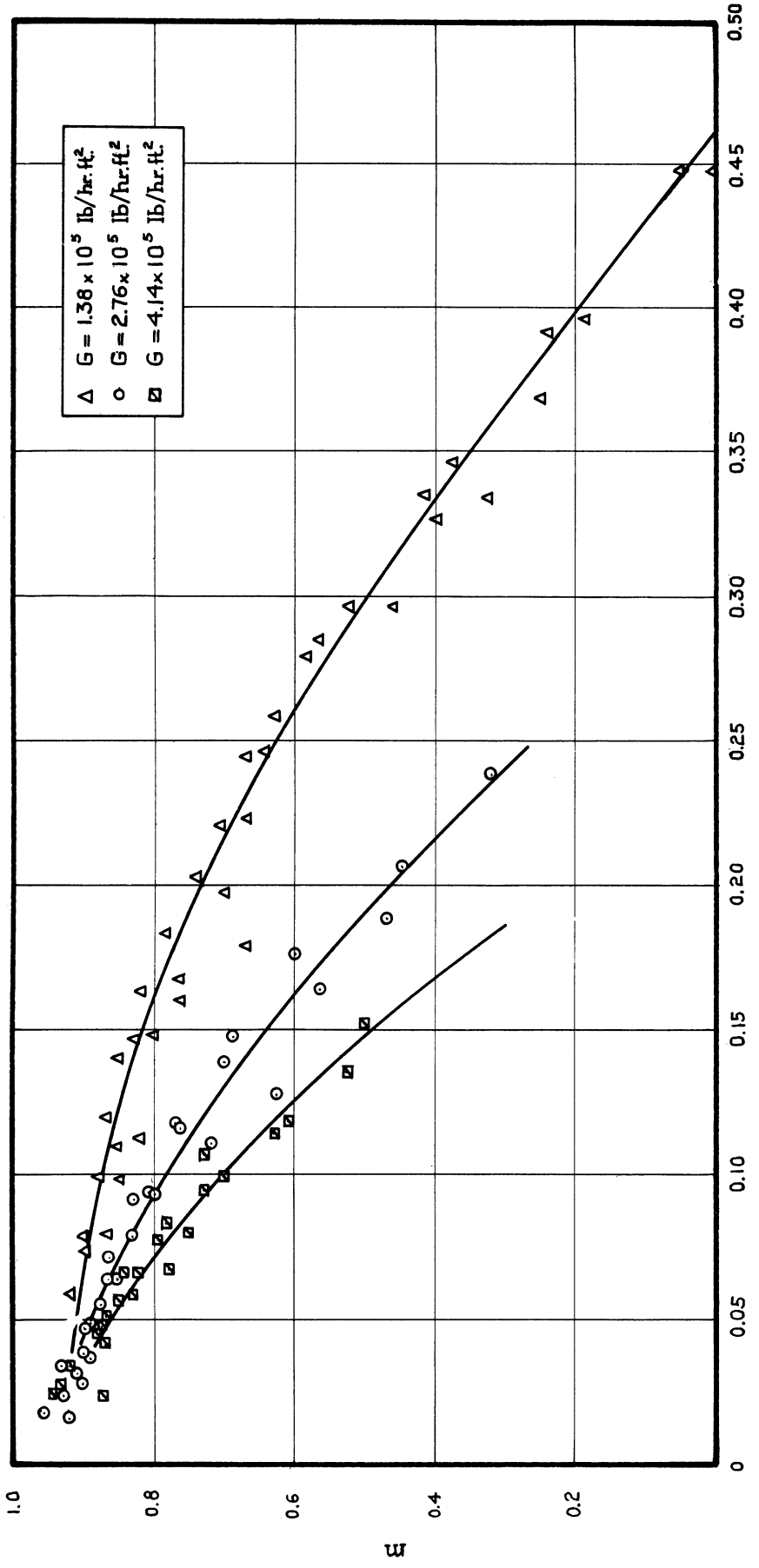

Figure 23. Coefficient m versus steam quality.

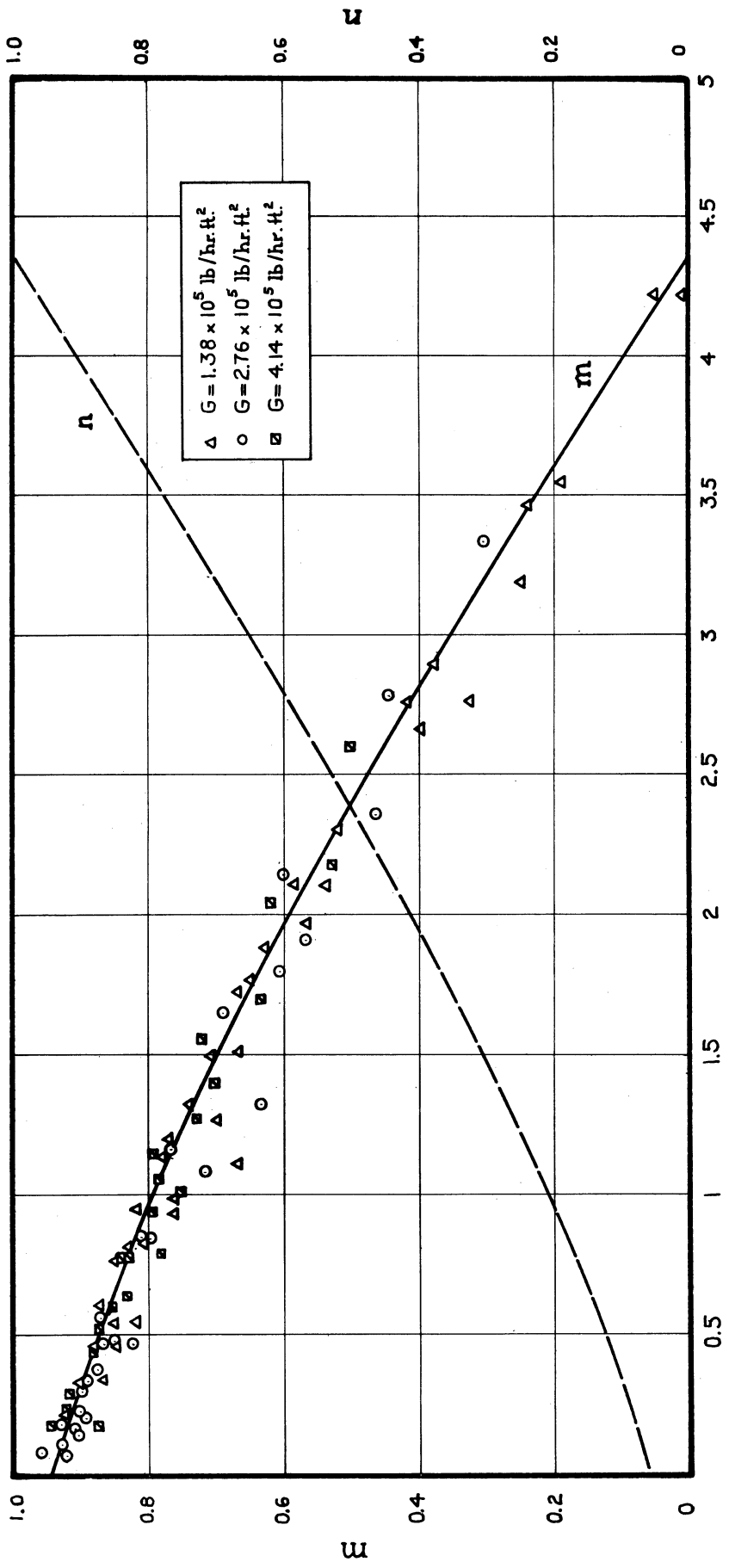

Figure 24. Coefficients m and n versus $10^{-4} \cdot \chi^{1.47} \cdot G$

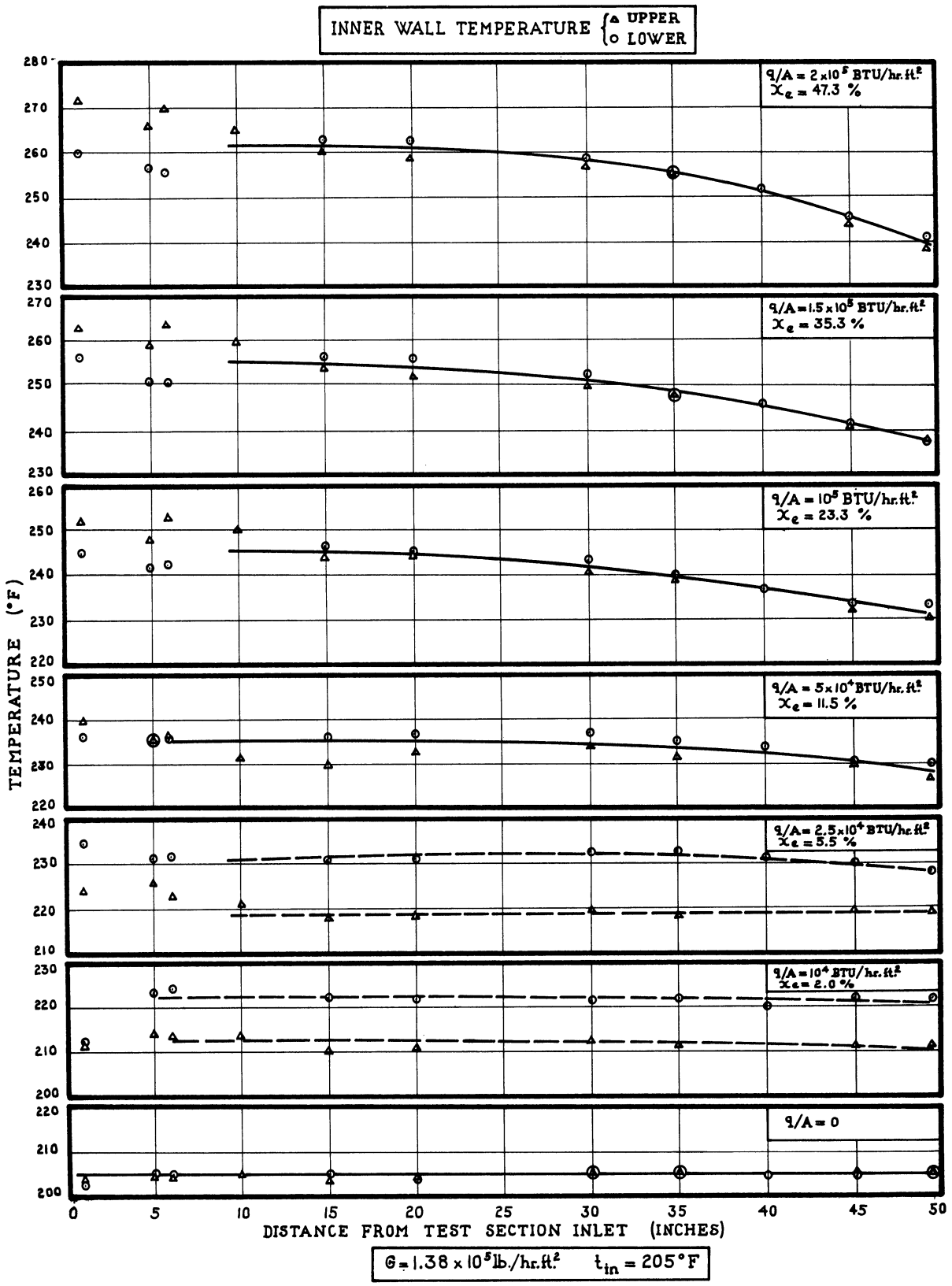

Figure 25. Inner Wall Temperatures for $G = 1.38 \times 10^5$ lb/hr ft^2, $t_{in} = 205^{\circ}$, $q/A = 0 - 2 \times 10^5$ BTU/hr ft^2

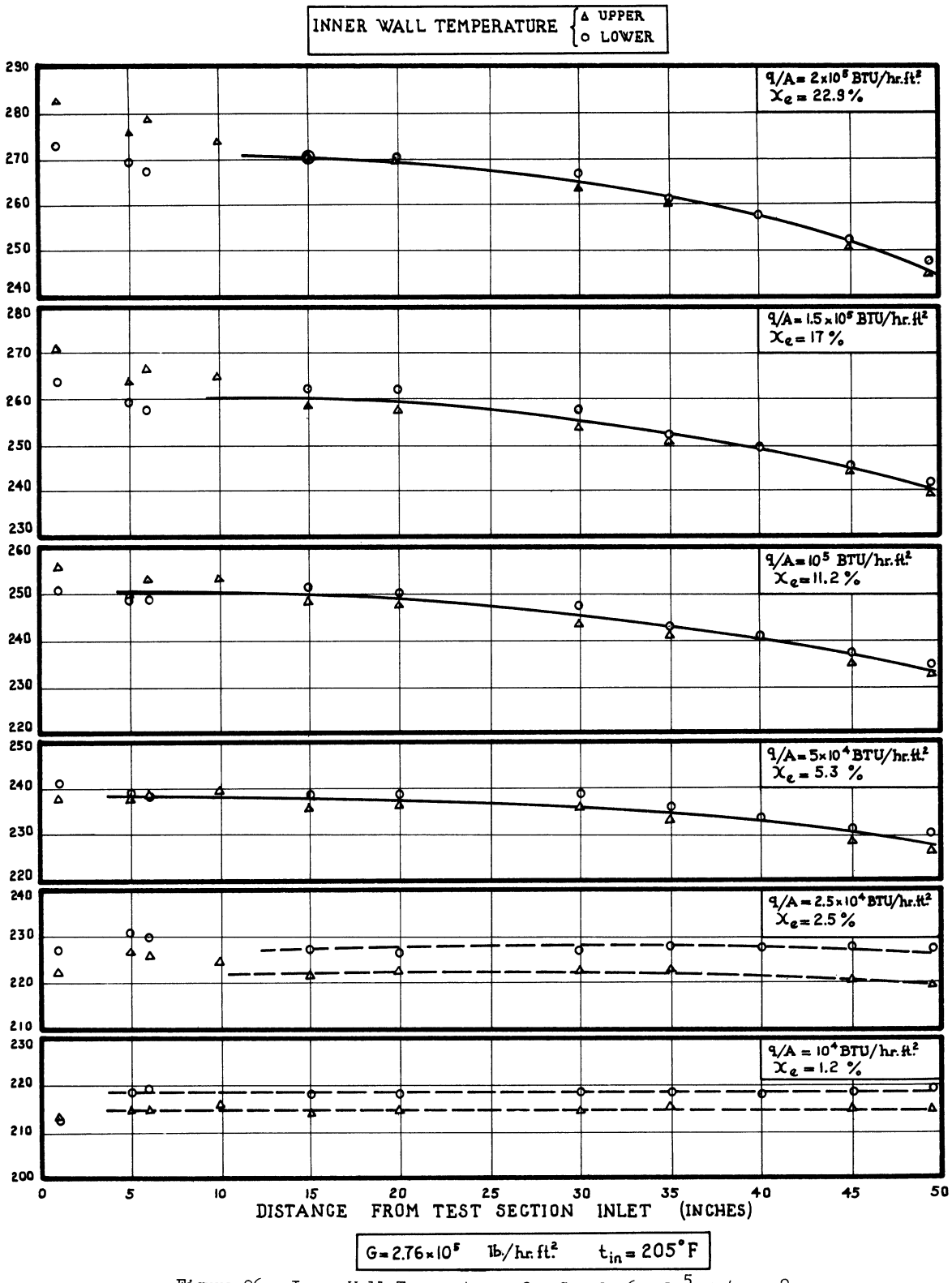

Figure 26. Inner Wall Temperatures for G = 2.76 x 10^5 lb/hr ft^2, t_{in} = 205°P, q/A = 10^4 - 2 x 10^5 BTU/hr ft^2

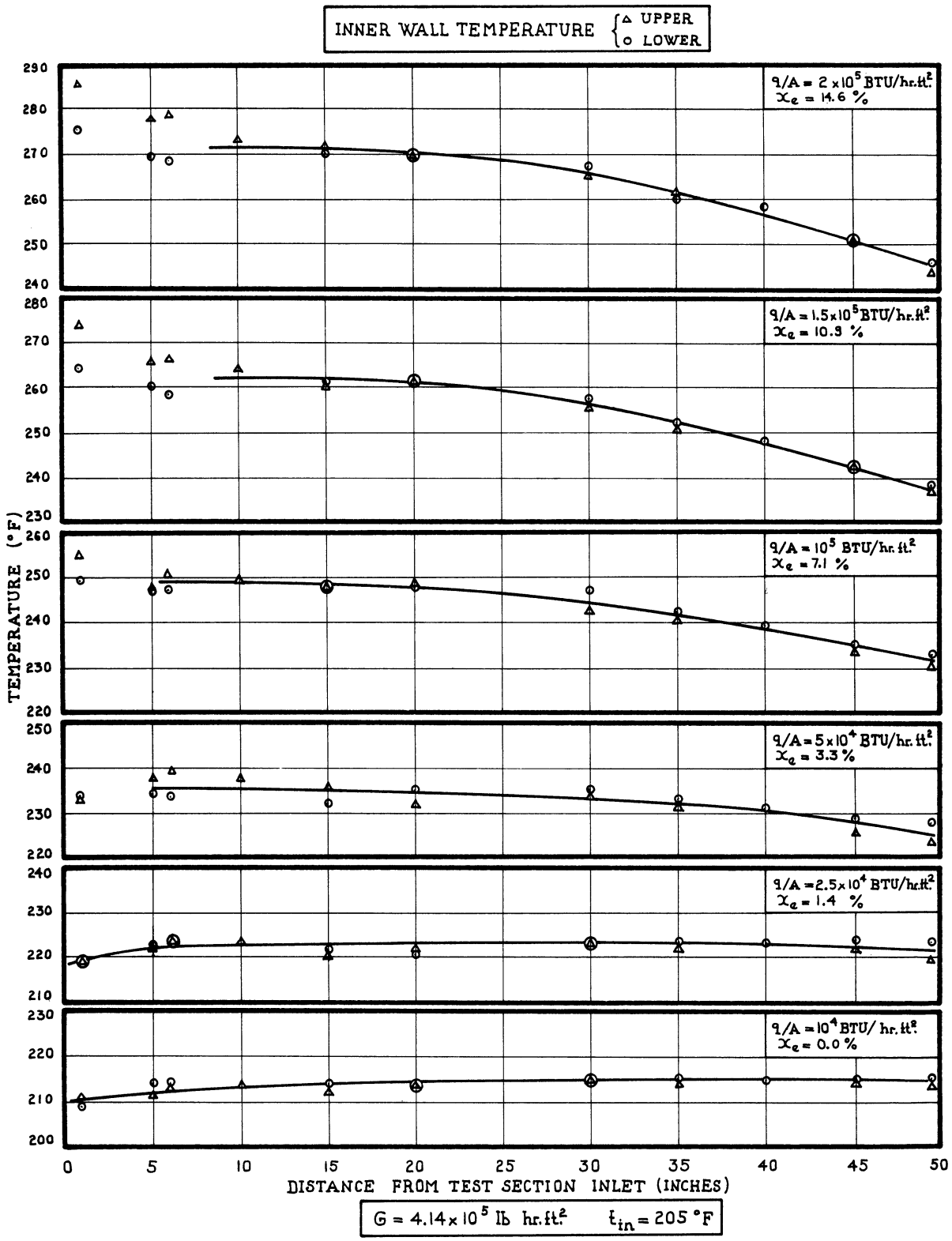

Figure 27. Inner Wall Temperatures for G = 4.14 x 10^5 lb/hr ft^2, t_{in} = 205°P, q/A = 10^4 - 2 x 10^5 BTU/hr ft^2

Figure 28.

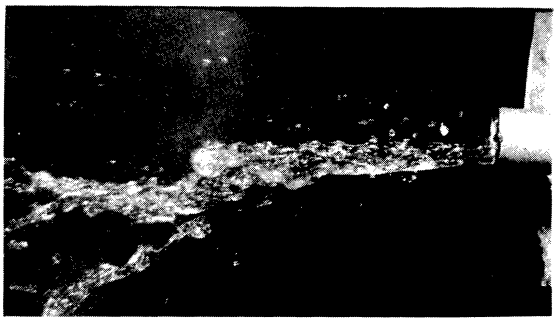

Figure 30.

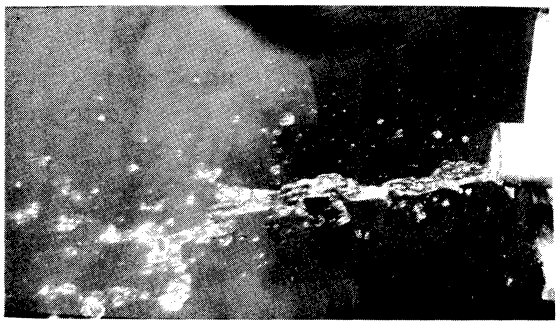

Figure 29.

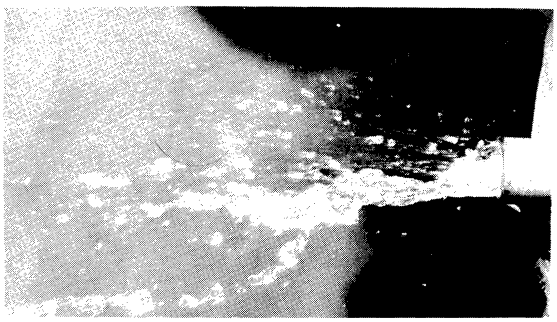

Figure 31.

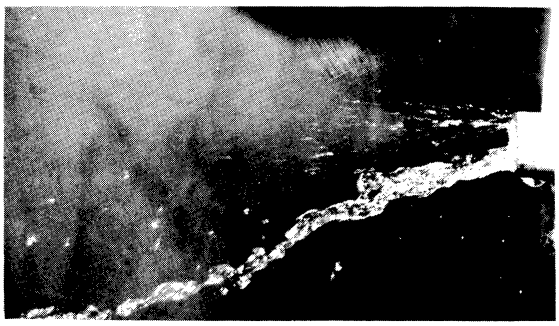

Figures 28 - 32. Photographs of Unsteady Stratified Slug Flow Patterns at the Test Section Outlet.
$G = 1.38 \times 10^5$ lb/hr ft^2, $X_e = 5.5\%$,
$q/A = 25{,}000$ Btu/hr ft^2

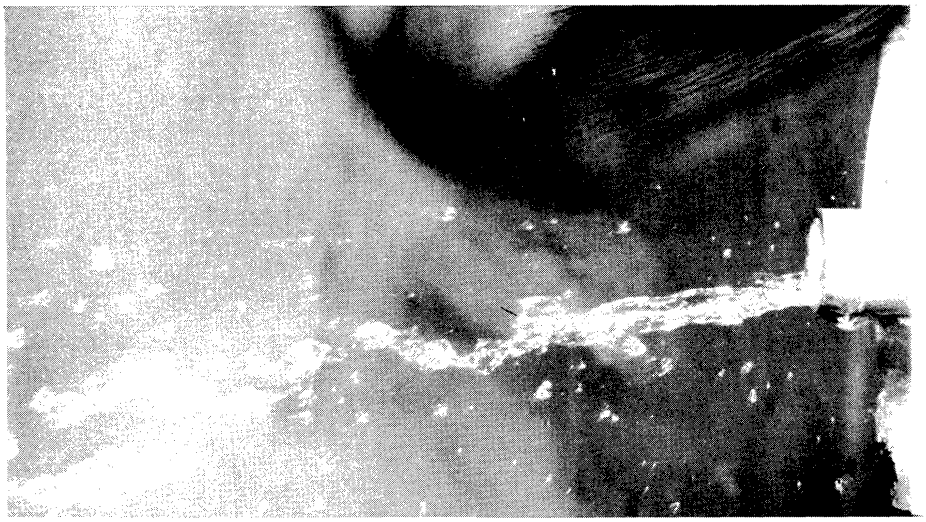

Figure 33.

Figures 33 - 34 Photographs of Unsteady Stratified Slug Flow Patterns at the Test Section Outlet $G = 2.76 \times 10^5$ lb/hr ft^2, $\chi_e = 2.5\%$, $q/A = 25{,}000$ Btu/hr ft^2

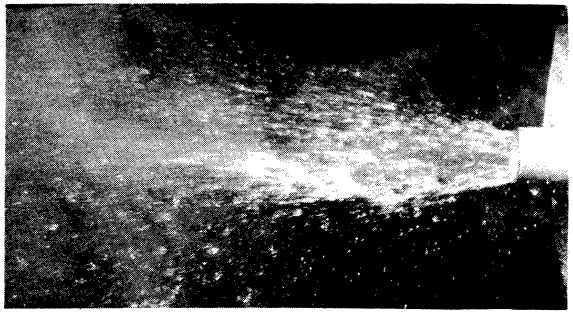

Figure 35. $G = 1.38 \times 10^5$ lb/hr ft^2, $\chi_e = 14\%$, $q/A = 61{,}000$ Btu/hr ft^2, $W = 290$ lb/hr

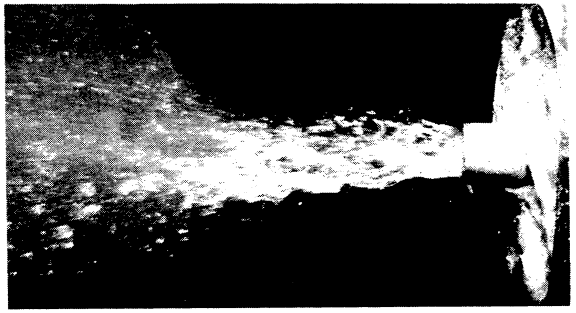

Figure 36. $G = 2.76 \times 10^5$ lb/hr ft^2, $\chi_e = 5.3\%$, $q/A = 50{,}000$ Btu/hr ft^2, $W = 580$ lb/hr

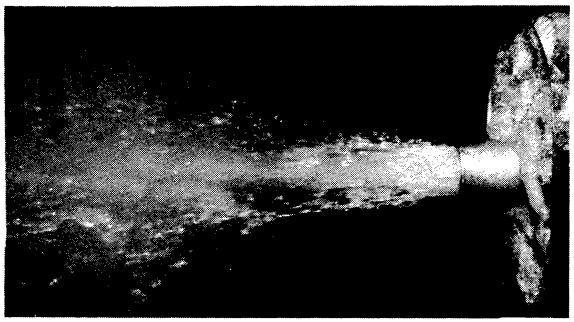

Figure 37. $G = 4.14 \times 10^5$ lb/hr ft^2, $\chi_e = 4\%$, $q/A = 61{,}000$ Btu/hr ft^2, $W = 870$ lb/hr

Figures 35 - 37 Photographs of Annular Flow Patterns at the Test Section Outlet.

Figure 38. $G = 1.38 \times 10^5$ lb/hr ft^2, $\chi_e = 29\%$, $q/A = 125{,}000$ Btu/hr ft^2, $W = 290$ lb/h

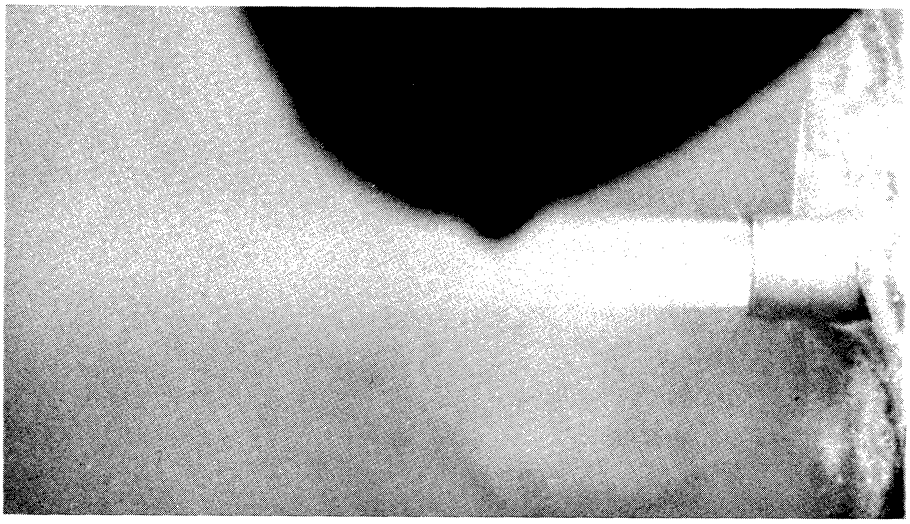

Figure 39. $G = 1.38 \times 10^5$ lb/hr ft^2, $\chi_e = 47\%$, $q/A = 200{,}000$ Btu/hr ft^2, $W = 290$ lb/hr

Figures 38 - 39. Photographs of Fog (or Liquid-dispersed) Flow Patterns at the Test Section Outlet

BIBLIOGRAPHY

1. Alves, G. E. "Co-Current Liquid Gas Flow in a Pipeline Contactor." Chem. Eng. Progress, 50, 449, (1954).

2. Baker, O. "Design of Pipelines for the Simultaneous Flow of Oil and Gas." The Oil and Gas Journal, July 26, 1954.

3. Galegar, W. C., Stovall, W. B., and Huntington, R. L. "More Data on Two-Phase Vertical Flow." Petroleum Refiner, 33, No. 11, 208-211, (1954).

4. Martinelli, R. C., Boelter, L. M. K., Taylor, T. H. M., Thomsen, E. G., and Morrin, E. H. "Isothermal Pressure Drop for Two-Phase Two-Component Flow in a Horizontal Pipe." Trans. Am. Soc. Mech. Engrs., 66, 139, (1944).

5. Dengler, C. E. Sc.D. Thesis in Chemical Engineering, Massachusetts Institute of Technology, 1952.

6. Dengler, C. E. and Addoms, J. N. "Heat Transfer Mechanism for Vaporization of Water in a Vertical Tube." Chemical Engineering Progress Symposium Series - "Heat Transfer-Louisville", 52, No. 18, 95 (1956).

7. Querrieri, S. A. and Talty, R. D. "A Study of Heat Transfer to Organic Liquids in Single-Tube Natural-Circulation Vertical-Tube Boilers." Chemical Engineering Progress Symposium Series - "Heat Transfer-Louisville", 52, No. 18, 69, (1956).

8. Jakob, M., Leppert, G., and Reynolds, J. B. "Pressure Drop During Forced-Circulation Boiling." Chemical Engineering Symposium Series - "Heat Transfer-Louisville", 52, No. 18, (1956).

9. Mumm, J. F. ANL 5276, (1954). BNL 2446, 103-109, (1955).

10. Coulson, J. M. and McNelly, M. J. Trans. Inst. Chem. Engrs., 74, 247-257, (1956).

11. Bennett, J. A. R., Collier, J. G., Pratt, H. R. C., and Thornton, J. D. "Steam-Water Mixtures in the Liquid Dispersed Region in an Annulus." AERC - R 3159, (1959).

12. Kreith, F. and Summerfield, M. Investigation of Heat Transfer at High Heat Flux Densities. Progress Report No. 4-68, Jet Propulsion Laboratory, California Institute of Technology, April 2, 1948.

13. Clark, J. A. Contribution to the discussion of Leppert, G., Costello, C. P. and Hoglund, B. M. "Boiling Heat Transfer to Water Containing a Volatile Additive." Trans. ASME, 80, 1395, (1958).

14. Lockhart, R. W. and Martinelli, R. C. "Proposed Correlation of Data for Isothermal Two-Phase, Two-Component Flow in Pipes." Chemical Engineering Progress, 45, 39, (1949).

15. Martinelli, R. C. and Nelson, D. B. "Prediction of Pressure Drop During Forced-Circulation Boiling of Water." Trans. ASME, 70 695, (1948).

16. Goldmann, K., Firstenberg, H., and Lombardi, C. Burnout in Turbulent Flow - A Droplet Diffusion Model. Presented at the ASME-AIChE Heat Transfer Conference, Buffalo, New York, Paper No. 60-HT-34, August 15-17, 1960.

17. Dickinson, N. L. and Welch, C. P. "Heat Transfer to Supercritical Water." Trans. ASME, 80, 746, (1958).